

Estimation of Synchronization Parameters

Jan-Jaap van de Beek

Part I

ML Estimation of Timing and Frequency Offset in Multicarrier Systems

This part has been published as
J.J. van de Beek, M. Sandell, P.O. Börjesson, 'ML Estimation of Timing and Frequency Offset in Multicarrier Systems', *Research Report TULEA 1996:09*, Division of Signal Processing, Luleå University of Technology.

This paper has been presented in part at the 1995 IEEE International Symposium on Synchronization, Saalbau, Essen, Germany, Dec. 14–15, 1995.

ML Estimation of Timing and Frequency Offset in Multicarrier Systems

J.J. van de Beek M. Sandell P.O. Börjesson

Div. of Signal Processing
Luleå University of Technology
S-971 87 Luleå, Sweden

Abstract – In this paper, we present a novel data-based method for simultaneous Maximum Likelihood (ML) symbol and carrier-frequency offset estimation in *Orthogonal frequency-division multiplexing* (OFDM) systems. Statistical properties introduced by the cyclic prefix, a guard space between OFDM symbols, provide sufficient information about the unknown parameters. It is shown that the redundancy introduced by this cyclic prefix allows the estimation to be performed without additional pilots. Simulations show that the performance of the frequency estimator is applicable in a tracking mode while the timing estimation can be used in an acquisition mode.

1 Introduction

Multi-carrier, or *Orthogonal frequency-division multiplexing* (OFDM), systems have gained an increased interest during the last years [1]. It is used in the European digital broadcast radio system [2] and its use in wireless applications such as digital broadcast television [3] and mobile communication systems [4] is currently being investigated. By the name of *discrete multitone* (DMT) modulation, OFDM is also being examined for broadband digital communication on existing copper networks. The OFDM technique has been proposed both for *high bit-rate digital subscriber lines* (HDSL) and *asymmetric digital subscriber lines* (ADSL) [5, 6].

In this paper we address two problems in the design of OFDM receivers. One problem is the unknown time instant to start sampling a new OFDM symbol. Sensitivity to a timing offset is higher in multi-carrier systems than in single-carrier systems and has been discussed in [7, 8]. A second problem is the mismatch of the oscillators in the transmitter and receiver. The demodulation of a signal with an offset in the carrier frequency can cause large bit errors and may degrade the performance of a symbol synchronizer [7, 9]. It is therefore important to estimate this offset and minimize its impact.

A symbol clock and a frequency offset estimate may be generated at the receiver with the aid of pilot symbols known to the receiver [10, 11], or, as in [12], by maximizing the average log-likelihood function. However, the structure of the transmitted OFDM signal itself offers the opportunity for synchronization. Such an approach is found in [11, 13] for a timing offset and in [14, 15] for a frequency offset. In this paper we present and evaluate the joint *Maximum Likelihood* (ML) estimation of the timing and carrier-frequency offset in OFDM systems. The key element that will rule the entire discussion is the idea that the OFDM data symbols contain sufficient information to perform synchronization [16]. The

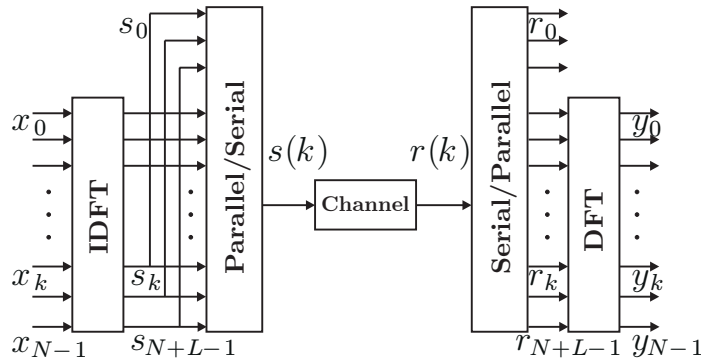


Figure 1: An OFDM system.

algorithm we present exploits the cyclic prefix preceding the OFDM symbols, commonly accepted as a means to mitigate *inter-symbol interference* (ISI) in OFDM systems [1, 17]. The need for pilots is thus reduced.

2 The OFDM system model

2.1 The signal model

Consider the transmission of complex numbers x_k , taken from some signal constellation (*e.g.*, PSK, QAM). Figure 1 illustrates the baseband, discrete-time OFDM system model we will use in the sequel.

The data x_k are modulated on N subcarriers by an inverse discrete Fourier transform (IDFT) and the last L samples are copied and put as a preamble (cyclic prefix) to form the OFDM symbol s_k . This data vector is serially transmitted over a discrete-time channel, whose impulse response is typically shorter than L samples. The cyclic prefix is removed at the receiver and the signal r_k is demodulated with a discrete Fourier transform (DFT). The insertion of a cyclic prefix avoids ISI and preserves the orthogonality between the tones, resulting in the simple input-output relation [1]

$$y_k = h_k x_k + n_k, \quad k = 0, \dots, N-1, \quad (1)$$

where h_k is the channel attenuation at the k^{th} subcarrier (See Figure 2) and n_k is additive white Gaussian noise. In spite of the loss of transmission power and bandwidth associated with the prefix, the simple channel equalization for the subchannel structure (1) generally motivates the use of the cyclic prefix [1].

In the following analysis, we assume that the channel is non-dispersive and that the transmitted signal $s(k)$ is only affected by complex, additive, white Gaussian noise (AWGN) $n(k)$ (*i.e.*, $h_k = 1, \forall k \in \{0, \dots, N-1\}$). In Section 5 we also evaluate the estimator performance for a time-dispersive channel.

We now consider two uncertainties in the receiver of this OFDM symbol. The uncertainty in the arrival time of the OFDM symbol is modelled as a delay in the channel impulse response, *i.e.*, $\delta(k - \theta)$, where θ is the integer-valued unknown arrival time of a

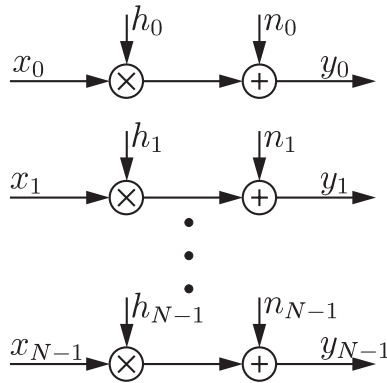


Figure 2: Equivalent model of the OFDM system.

symbol. The uncertainty in carrier frequency, which is due to a difference in the local oscillators in the transmitter and receiver, gives rise to a shift in the frequency domain. Such behaviour is modelled as a complex multiplicative distortion in the time domain, $e^{j2\pi\varepsilon k/N}$, of the received data, where ε denotes the difference in the transmitter and receiver oscillators as a fraction of the inter-carrier spacing. Hence, the received data is

$$r(k) = s(k - \theta)e^{j2\pi\varepsilon k/N} + n(k). \quad (2)$$

Now consider the transmitted signal $s(k)$. This is the DFT of the data x_k , which we assume constitutes a white process. Hence, $s(k)$ is a linear combination of independent, identically distributed random variables. If the number of subcarriers is sufficiently large, we know from the central limit theorem that $s(k)$ approximates a complex Gaussian process whose real and imaginary parts are independent. This process, however, is not white, since the appearance of a cyclic prefix yields a correlation between some pairs of samples, spaced N samples apart. Hence, $r(k)$ is not a white process, either, but because of its probabilistic structure, it contains information about the timing offset θ and carrier frequency offset ε . This is the crucial observation that offers the opportunity for simultaneous estimation of these parameters based on $r(k)$. In the following sections, this idea is formally shaped and elaborated.

2.2 Sensitivity for timing and frequency offset

A synchronizer cannot distinguish between phase shifts introduced by the channel and those introduced by symbol timing delays [8]. Depending on the application, this interchangeability affects the requirements with respect to timing synchronization differently. In wireless applications, where channel estimation is performed continuously in order to track a time-varying channel, timing errors can be corrected by the equalizer. In these cases, it may be sufficient that the accuracy of the timing synchronizer is in the order of one sample. In, *e.g.*, HDSL, however, the channel is static and essentially estimated only during start-up. Any timing error gives rise to a phase shift of the channel attenuations h_k . If the constellation size of the transmitted symbols x_k is large, the demands can be rather high.

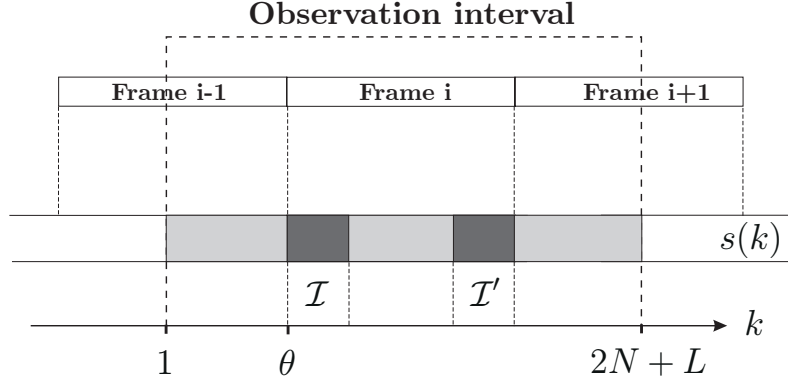


Figure 3: Structure of OFDM signal with cyclicly extended symbols, $s(k)$.

The frequency response of each subchannel is zero at all other subcarrier frequencies; *i.e.*, the subchannels don't interfere with each other [1]. The effect of a frequency offset is a translation of these frequency responses resulting in a loss of orthogonality between the tones. This inter-carrier interference (ICI) has been investigated in [14]. The signal-to-interference ratio (SIR) is shown to be lower bounded by

$$\text{SIR} \geq \frac{1}{0.5947\pi^2\varepsilon^2}. \quad (3)$$

Notice that additive noise is not incorporated in this analysis. To obtain a SIR of 30 dB or higher, the frequency offset must satisfy

$$\varepsilon \leq 1.3 \cdot 10^{-2}. \quad (4)$$

This result agrees well with the analysis of multi-user OFDM systems in [7], which states that a frequency accuracy of 1%–2% of the inter-carrier spacing is necessary.

2.3 Correlation properties

Assume that we observe $2N+L$ consecutive samples of $r(k)$, *cf.* Figure 3, and that these samples contain one complete $(N+L)$ -sample OFDM symbol. The position of this symbol within the observed block of samples, however, is unknown because the channel delay θ is unknown to the receiver. Define the index sets $\mathcal{I} \equiv \{\theta, \dots, \theta + L - 1\}$ and $\mathcal{I}' \equiv \{\theta + N, \dots, \theta + N + L - 1\}$, see Figure 3. The set \mathcal{I}' thus contains the indexes of the data samples that are copied into the cyclic prefix, and the set \mathcal{I} contains the indexes of this prefix. Collect the observed samples in the $(2N+L) \times 1$ -vector

$$\mathbf{r} \equiv [r(1) \dots r(2N+L)]^T. \quad (5)$$

Notice that the samples in the cyclic prefix and their copies, $r(k)$, $k \in \mathcal{I} \cup \mathcal{I}'$ are pairwise correlated, *i.e.*, $\forall k \in \mathcal{I}$:

$$E \{r(k)r^*(k+m)\} = \begin{cases} \sigma_s^2 + \sigma_n^2 & m = 0 \\ \sigma_s^2 e^{j2\pi\varepsilon} & m = N \\ 0 & \text{otherwise,} \end{cases} \quad (6)$$

where $\sigma_s^2 \equiv E \{ |s(k)|^2 \}$ and $\sigma_n^2 \equiv E \{ |n(k)|^2 \}$, while the remaining samples $r(k), k \notin \mathcal{I} \cup \mathcal{I}'$ are mutually uncorrelated. In the next Section we explicitly exploit this correlation property and derive the ML estimates of θ and ε .

3 Maximum Likelihood estimation

3.1 The likelihood function

The log-likelihood function for θ and ε , $\Lambda(\theta, \varepsilon)$, is the logarithm of the probability density function $f(\mathbf{r}|\theta, \varepsilon)$ of the $2N + L$ observed samples in \mathbf{r} given the arrival time θ and the carrier frequency offset ε , *i.e.*,

$$\Lambda(\theta, \varepsilon) = \log f(\mathbf{r}|\theta, \varepsilon). \quad (7)$$

In the following, we will drop all additive and (positive) multiplicative constants that show up in the expression of the log-likelihood function, since they don't affect the maximizing argument. Any such scaling of $\Lambda(\theta, \varepsilon)$ will be referred to with the same notation. Moreover, we drop the conditioning on (θ, ε) for clarity and use the correlation properties of the observations \mathbf{r} . As in [18], the log-likelihood function (7) can be written as

$$\begin{aligned} \Lambda(\theta, \varepsilon) &= \log \left(\prod_{k \in \mathcal{I}} f(r(k), r(k+N)) \prod_{k \notin \mathcal{I} \cup \mathcal{I}'} f(r(k)) \right) \\ &= \log \left(\prod_{k \in \mathcal{I}} \frac{f(r(k), r(k+N))}{f(r(k)) f(r(k+N))} \prod_k f(r(k)) \right), \end{aligned} \quad (8)$$

where $f(\cdot)$ denotes the probability density function of the variables in the argument. Notice that it is used for both one- and two-dimensional distributions. The last factor in (8) is independent of θ (since the product is over all k) and ε (since the real and imaginary parts of $r(k)$ are independent). The *maximum likelihood* (ML) estimation of θ and ε is the argument maximizing $\Lambda(\theta, \varepsilon)$. Hence, we may omit this factor and write the log-likelihood function as

$$\Lambda(\theta, \varepsilon) = \log \left(\prod_{k=\theta}^{\theta+L-1} \frac{f(r(k), r(k+N))}{f(r(k)) f(r(k+N))} \right). \quad (9)$$

Under the assumption that \mathbf{r} is a jointly Gaussian vector, this function is shown in the first Appendix to be

$$\Lambda(\theta, \varepsilon) = |\gamma(\theta)| \cos(2\pi\varepsilon + \angle\gamma(\theta)) - \rho\mathcal{E}(\theta), \quad (10)$$

where \angle denotes the argument of a complex number,

$$\gamma(m) \equiv \sum_{k=m}^{m+L-1} r(k)r^*(k+N), \quad (11)$$

$$\mathcal{E}(m) \equiv \frac{1}{2} \sum_{k=m}^{m+L-1} |r(k)|^2 + |r(k+N)|^2, \quad (12)$$

and

$$\rho \equiv \frac{\sigma_s^2}{\sigma_s^2 + \sigma_n^2} = \frac{\text{SNR}}{\text{SNR} + 1} \quad (13)$$

is the magnitude of the correlation coefficient between $r(k)$ and $r(k+N)$. SNR denotes the *Signal-to-Noise Ratio* and is defined as σ_s^2/σ_n^2 . The first term in (10) is the weighted magnitude of the sum of the correlation between L consecutive pairs of samples. It contributes positively to the log-likelihood function. This contribution is weighted by a factor depending on the frequency offset. The term $\mathcal{E}(\theta)$ is an energy term, independent of the frequency offset ε , and contributes negatively to the log-likelihood function. Notice that this contribution is SNR-dependent (by the weighting-factor ρ).

3.2 Simultaneous estimation

The calculation of the ML-estimates, *i.e.*, the maximization of the log-likelihood function, can be performed in two steps:

$$\max_{(\theta, \varepsilon)} \Lambda(\theta, \varepsilon) = \max_{\theta} \max_{\varepsilon} \Lambda(\theta, \varepsilon) = \max_{\theta} \Lambda(\theta, \hat{\varepsilon}_{\text{ML}}(\theta)). \quad (14)$$

The maximum with respect to the frequency offset ε is obtained when the cosine-term in (10) equals one, *i.e.*, when

$$2\pi\varepsilon + \angle\gamma(\theta) = n \cdot 2\pi, \quad (15)$$

where n is an integer. This yields

$$\hat{\varepsilon}_{\text{ML}}(\theta) = -\frac{1}{2\pi} \angle\gamma(\theta) + n. \quad (16)$$

A similar frequency offset estimator has been derived in [14] under different assumptions. Notice that by the periodicity of the cosine function, several maxima are found. We assume that an acquisition, or rough estimate, of the frequency offset has been performed and that $|\varepsilon| < 1/2$. Since

$$\cos(2\pi\hat{\varepsilon}_{\text{ML}}(\theta) + \angle\gamma(\theta)) = 1, \quad (17)$$

the log-likelihood function of θ (the compressed log-likelihood function with respect to ε) becomes

$$\Lambda(\theta, \hat{\varepsilon}_{\text{ML}}(\theta)) = |\gamma(\theta)| - \rho\mathcal{E}(\theta) \quad (18)$$

and the simultaneous ML-estimation of θ and ε becomes

$$\hat{\theta}_{\text{ML}} = \arg \max_{\theta} \{|\gamma(\theta)| - \rho\mathcal{E}(\theta)\} \quad (19)$$

$$\hat{\varepsilon}_{\text{ML}} = -\frac{1}{2\pi} \angle\gamma(\hat{\theta}_{\text{ML}}). \quad (20)$$

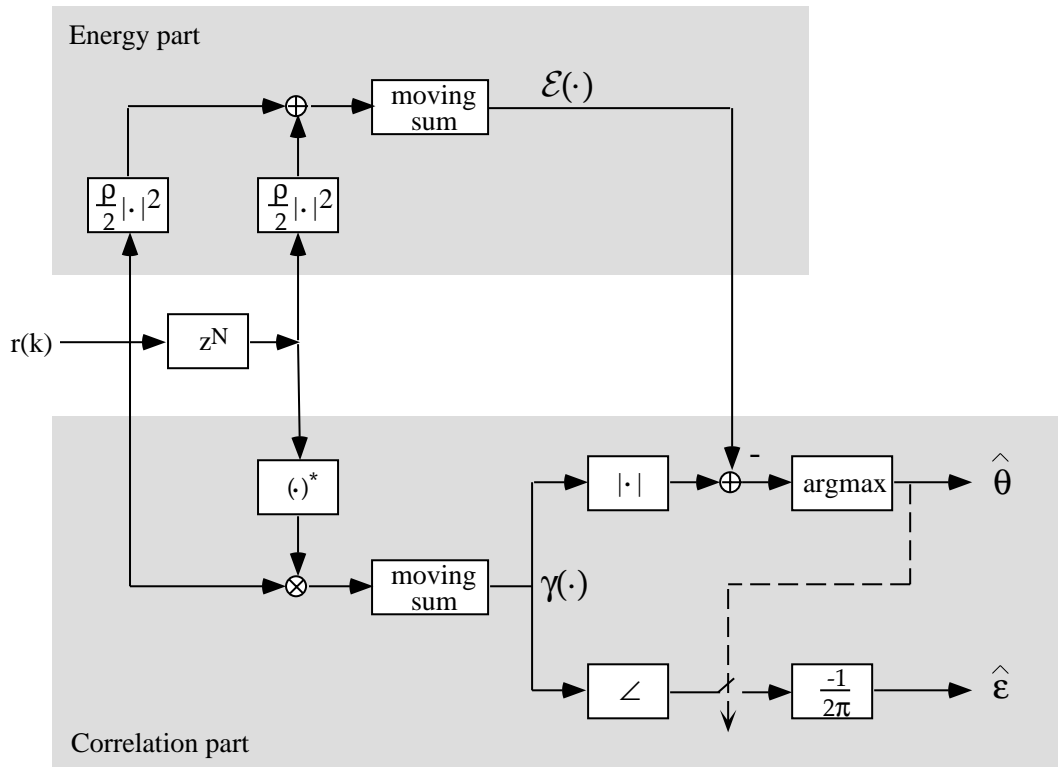


Figure 4: Block scheme of the ML estimator.

Notice that only two quantities affect the shape of the log-likelihood function (and thus the performance of the estimator): the number of samples in the cyclic prefix, L , and the correlation coefficient ρ given by the signal-to-noise ratio. Consequently, these parameters are assumed to be known at the receiver. This is no constraining assumption for the parameter L which always is known. The SNR, however, is usually not known at the receiver and must be fixed or estimated. Basically, the quantity $\gamma(\theta)$ provides the estimates of θ and ε . Its phase is proportional to ε , while its magnitude, compensated by an energy term, peaks at time instant θ . If ε is *a priori* known to be zero, *i.e.*, we only estimate θ , the log-likelihood function for θ becomes $\Lambda(\theta) = \text{Re}\{\gamma(\theta)\} - \rho\mathcal{E}(\theta)$ and $\hat{\theta}_{\text{ML}}$ is its maximizing argument. This estimator and a low-complex variant is analyzed in [13].

4 Synchronization

A block scheme of the ML timing and frequency estimator is shown in Figure 4. $2N + L$ samples of the received signal $r(k)$ are stored in a buffer and $\gamma(\theta)$, defined in (11), is calculated on-line. Figure 5 shows $\Lambda(\theta, \hat{\varepsilon}_{\text{ML}}(\theta))$, defined in (18), and whose maximizing arguments are the timing estimates $\hat{\theta}_{\text{ML}}$ and $-(1/2\pi)\angle\gamma(\theta)$, whose values at the time instants $\hat{\theta}_{\text{ML}}$ yield the frequency estimates. Notice that Figure 4 depicts an open-loop structure. Closed-loop implementations based on (10) and (18) may also be considered. In such structures the signal $\Lambda(\theta, \hat{\varepsilon}_{\text{ML}}(\theta))$ is typically input to a *Phase Locked Loop* (PLL),

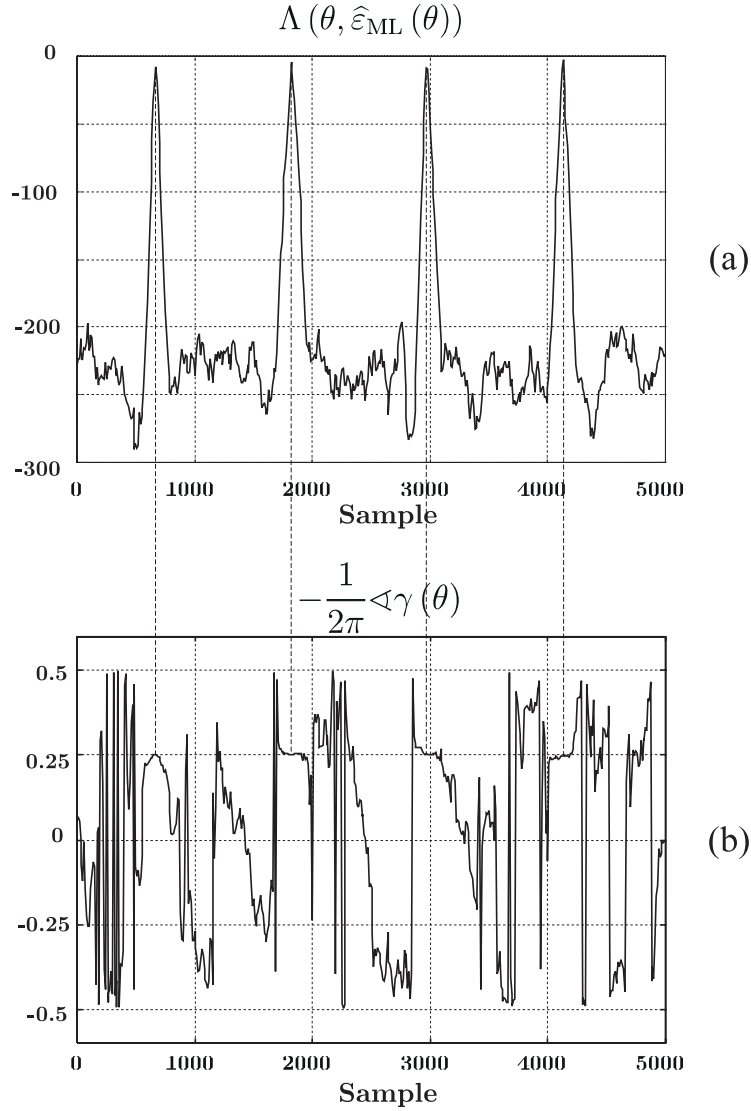


Figure 5: The signals that generate the ML-estimates ($N = 1024$, $L = 128$, $\varepsilon = 0.25$ and SNR= 15 dB): *a)* The maximums of $\Lambda(\theta, \hat{\varepsilon}_{\text{ML}}(\theta))$ give the timing estimate $\hat{\theta}_{\text{ML}}$. *b)* At these time instants the argument of $\gamma(\theta)$ gives $\hat{\varepsilon}_{\text{ML}}$.

generating a stable clock.

The estimation can be improved if the parameters θ and ε can be considered constant over several OFDM symbols. Assume that the observation containing M complete OFDM symbols consists of $M(N + L) + N$ samples. In the second Appendix it is shown that the log-likelihood function of this observation is

$$\Lambda(\theta, \varepsilon) = \sum_{m=0}^{M-1} \Lambda_m(\theta, \varepsilon), \quad (21)$$

where $\Lambda_m(\theta, \varepsilon)$ is the log-likelihood function of symbol m as described in (7). Thus, to obtain the log-likelihood function we may sum the log-likelihood functions of the

individual symbols. Notice that this result is the same as in the situation where the individual observation intervals are independent. Since the observation intervals overlap, they are not independent, but this does not affect the optimal estimation.

Two considerations affect the choice of M , and thus the number of received samples to process simultaneously. First, the allowed complexity in the receiver may bound the choice of M . Second, the nature of the physical channel determines how long the arrival time θ and the frequency offset ε can be assumed to be constant. Estimator (21) is not the optimal ML-estimation if this assumption is violated. Simply averaging the estimations themselves, for instance, may yield better estimates in terms of error variance.

5 Simulations

We have performed Monte Carlo simulations to evaluate the performances of the suggested synchronization algorithms. First, the performance for the AWGN channel is presented. These results show the potential of the estimation methods and give a lower bound on the performance of the methods applied to dispersive channels. Moreover, they illustrate and provide insight about some basic properties of non-linear estimators.

Furthermore, an outdoor fading radio channel environment for OFDM is simulated. Since this environment suffers from time dispersion, the estimators are not optimal. Moreover, fading radio channels introduce a time-variant arrival time. This arrival time varies depending on the relative Doppler. This readily limits the usefulness of the averaging estimator. We present simulations of a slowly fading radio channel, allowing for moderate averaging

In the fading channel the definition of θ is not obvious. In this case the variance of the estimator is a more suitable performance measure than the mean-squared error. Since simulations show that the estimators are unbiased for the AWGN channel, *i.e.*, estimator variance equals mean-squared error, we evaluate the performance of the estimators in both environments, using the estimator variance. Practically, this performance measure shows the ability of the estimators to track variations of the parameters.

5.1 AWGN channel

As mentioned in Section 3, the log-likelihood function depends on the length of the cyclic prefix, L , and the system SNR. In order to investigate how these parameters affect the estimator performance, we consider an OFDM system with 256 subcarriers and an additive white, complex Gaussian noise channel.

First, the estimator error variance as a function of L , is estimated. For each value of L , 50,000 symbols are simulated. Results, not shown in the Figures, show that the error variances of $\hat{\theta}$ and $\hat{\varepsilon}$ are independent of the actual values of θ and ε . Figure 6 shows the estimator performance for SNR values of 4 dB, 10 dB and 16 dB. Notice that the timing estimator performance is independent of L , provided that the cyclic prefix is longer than a certain threshold value. This value decreases with the SNR. Thus, for the AWGN channel and from a time synchronization viewpoint, there is no need to increase the length of the cyclic prefix beyond this threshold value. A similar threshold appears

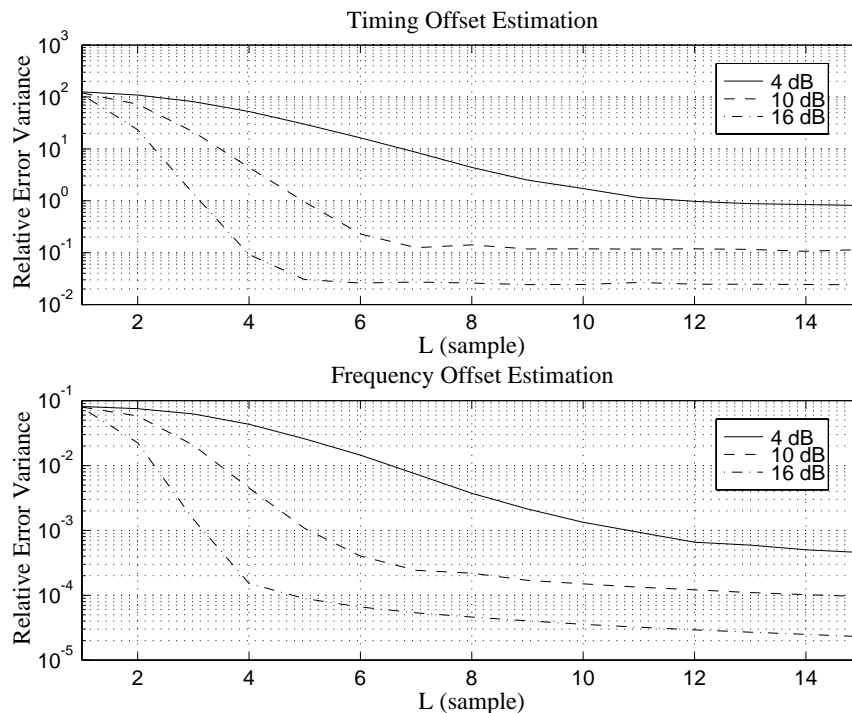


Figure 6: Performance of the timing (top) and frequency (bottom) estimators for the AWGN channel for 4 dB, 10 dB, and 16 dB. The number of subcarriers is $N = 256$.

for the frequency estimator, but above this threshold the error variance still decreases. We will discuss this property in Section 6.

Furthermore, the estimator variances as a function of SNR for $L = 4$, $L = 6$, and $L = 8$ are shown in Figure 7. These curves show the potential of the estimators and give insight into some of their properties. Notice, for example, that a similar threshold phenomenon as in Figure 6 occurs even in these plots. This phenomenon is a property of time delay estimation and is documented in, *e.g.*, [19].

5.2 Fading channel

The results in the previous Section show the estimator performance for the AWGN channel, which does not introduce inter-symbol interference, and consequently does not prompt for a cyclic prefix. Although the results for this channel provide insight into the estimation methods, they do not directly apply to dispersive channels. We now consider the performance of the estimators in a time dispersive channel environment.

A wireless system operating at 2 GHz with a bandwidth of 5 MHz is simulated. In these simulations, an OFDM symbol consists of 256 subcarriers. An outdoor fading environment with additive white Gaussian noise and micro-cell characteristics is chosen: the channel has an exponentially decaying power delay spread with rms-value equal to $0.4 \mu\text{s}$ (corresponding to 2 samples) and a maximum delay spread of $2\text{--}3 \mu\text{s}$ (corresponding to 10–15 samples). It is modelled to consist of 15 independent Rayleigh-fading taps [20].

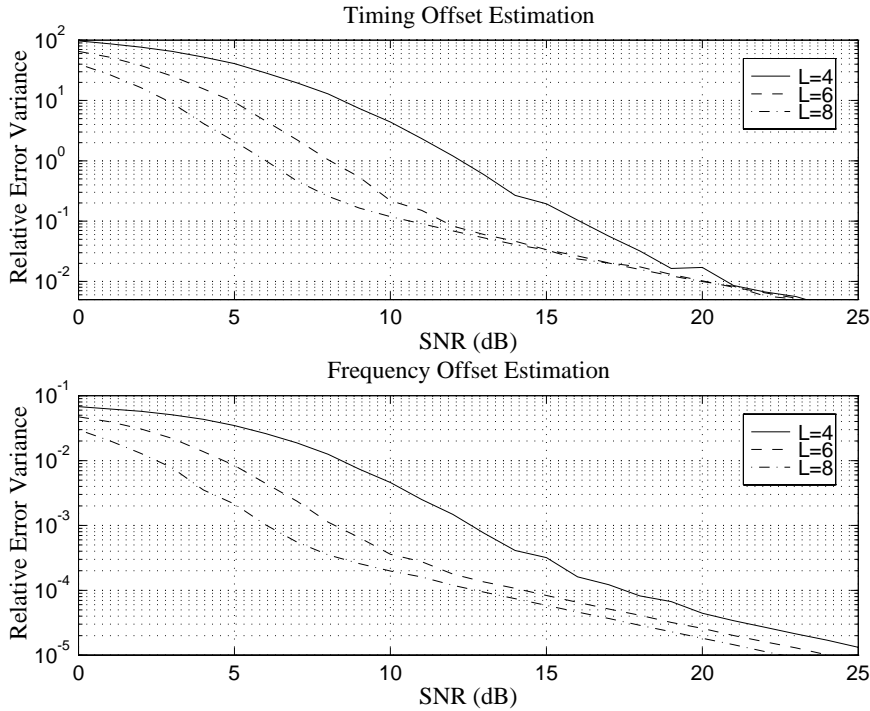


Figure 7: Performance of the timing (top) and frequency (bottom) estimators for the AWGN channel for $L = 4$, $L = 6$, and $L = 8$. The number of subcarriers is $N = 256$.

We choose the cyclic prefix to consist of 15 samples. This choice avoids ISI, while the loss of power and bandwidth due to the cyclic prefix ($L/(N + L)$) is about 5%.

The mobile is assumed to be moving at a maximum speed of 50 km/h, resulting in a maximum Doppler frequency of 100 Hz (0.5% maximum Doppler, normalized to the intercarrier spacing). This Doppler frequency is small enough to motivate the averaging of 8 symbols in the synchronization algorithm, since the channel impulse response does not change significantly during this interval. This system transmits about 18,000 OFDM symbols per second, each containing 256 complex information symbols.

Figure 8 clearly shows the performance degradation caused by the dispersive channel as compared to the corresponding curves for the AWGN channel (Figure 7). The estimators operate in an environment for which they are not designed and consequently are not optimal. The fading channel introduces an error floor which is reached at approximately 15 dB. It is noteworthy that the averaging effect is lower here than for the AWGN channel, actually less than a factor 8 for some SNR values. Hence, it may be better to average after peak detection, *i.e.*, the actual estimation values, which, as a beneficial side effect, decreases the complexity of the estimators.

As was discussed in Section 2, a time delay is interchangeable with the channel phase. Depending on the application and the presence of a high performance channel estimator/equalizer, the performance of the timing estimate, as seen in Figure 8 (standard deviation of 1–2 samples) may be good enough to generate a stable clock. In most situations this performance will suffice in an acquisition mode. The frequency offset estimator

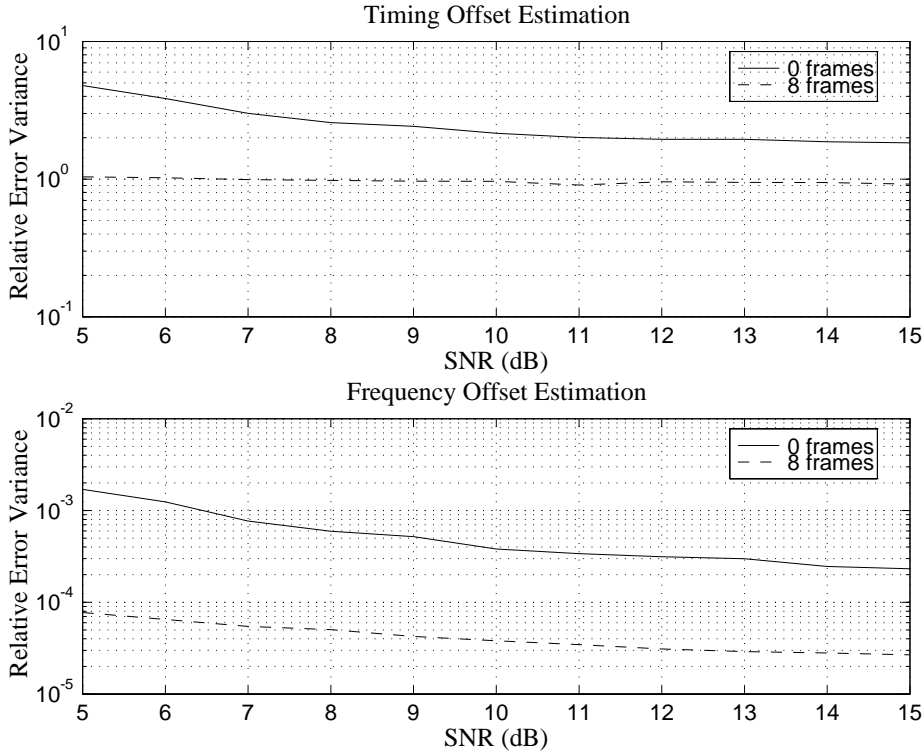


Figure 8: Performance of the timing estimator (top) and the frequency estimator (bottom) for the fading channel. The upper curves are without averaging and the lower are with 8 symbols averaging. The number of subcarriers is $N = 256$

shows an error standard deviation of less than 1% of the inter-tone spacing, see Figure 8. This is below the requirements found in [7] for multi-user OFDM systems.

6 Discussion

In this paper we have presented a simultaneous estimator of timing and frequency offset in OFDM systems. This estimator does not need pilots, but uses the redundancy introduced by the cyclic prefix. It is derived under the assumption that the channel only consists of additive noise but simulations show that it can perform well with a dispersive channel. An ML estimator for the latter case may be derived, but it will not have the same simple structure as the proposed estimator. For the AWGN channel, only samples in the cyclic prefix and their copies will be correlated, but signals passed through a dispersive channel will not have this structure.

The reason for the superior performance of the frequency estimator over the timing estimator, is an implicit averaging. As seen in (16) and (11), the estimate is the argument of a sum of complex numbers. With no additive noise $n(k)$, each term $r(k)r^*(k+N)$ has the same argument, $-2\pi\varepsilon$. Hence, they contribute coherently to the sum, while the additive noise contributes incoherently. This implies that the performance will be better with increasing size of the cyclic prefix.

In a wireless system, pilots are needed for channel estimation. These known symbols can be used by the timing estimator in the synchronizer and hence further increase the performance. Resulting synchronizers may be hybrid structures using both pilots and the redundancy of the cyclic prefix. How to incorporate pilot symbols in such timing and frequency estimators is not straightforward and needs further research.

Acknowledgement

The authors wish to thank Telia Research AB for the fruitful co-operation, in particular Mikael Isaksson for useful contributions, discussions and suggestions.

The log-likelihood function

For all $k \in \{\theta, \dots, \theta + L - 1\}$, define the complex-valued vector

$$\mathbf{x} = \begin{bmatrix} x_1 \\ x_2 \end{bmatrix} \equiv \begin{bmatrix} r(k) \\ r(k + N) \end{bmatrix}. \quad (22)$$

With the signal model described in Section 2, we have, since $x_1 = r(k)$ belongs to the cyclic prefix,

$$\begin{aligned} E \{x_1 x_1^*\} &= E \{x_2 x_2^*\} = \sigma_s^2 + \sigma_n^2, \\ E \{x_1 x_2^*\} &= E \{x_1^* x_2\}^* = \sigma_s^2 e^{-j2\pi\varepsilon}, \end{aligned}$$

where $\sigma_s^2 \equiv E \{|s(k)|^2\}$ and $\sigma_n^2 \equiv E \{|n(k)|^2\}$ are the variances of s and n , respectively. The log-likelihood function (9) can now be written as

$$\Lambda(\theta, \varepsilon) = \sum_{k=\theta}^{\theta+L-1} \log \left(\frac{f(\mathbf{x})}{f(x_1) f(x_2)} \right). \quad (23)$$

The nominator is a two-dimensional complex-valued Gaussian distribution

$$f(\mathbf{x}) = \frac{\exp \left(-\frac{|x_1|^2 - 2\rho \operatorname{Re}\{e^{j2\pi\varepsilon} x_1 x_2^*\} + |x_2|^2}{(\sigma_s^2 + \sigma_n^2)(1 - \rho^2)} \right)}{\pi^2 (\sigma_s^2 + \sigma_n^2)^2 (1 - \rho^2)}, \quad (24)$$

where

$$\rho \equiv \left| \frac{E \{r(k) r^*(k + N)\}}{\sqrt{E \{|r(k)|^2\} E \{|r(k + N)|^2\}}} \right| = \frac{\sigma_s^2}{\sigma_s^2 + \sigma_n^2} \quad (25)$$

is the magnitude of the correlation coefficient between $r(k)$ and $r(k + N)$. The denominator of (23) consists of two one-dimensional complex Gaussian distributions and the

log-likelihood function (23) becomes

$$\begin{aligned}
\Lambda(\theta, \varepsilon) &= \\
&= \sum_{k=\theta-L+1}^{\theta} \log \left(\frac{\exp \left(-\frac{|x_1|^2 - 2\rho \operatorname{Re}\{e^{j2\pi\varepsilon} x_1 x_2^*\} + |x_2|^2}{(\sigma_s^2 + \sigma_n^2)(1-\rho^2)} \right)}{\pi^2 (\sigma_s^2 + \sigma_n^2)^2 (1-\rho^2)} \frac{\pi (\sigma_s^2 + \sigma_n^2)}{\exp \left(-\frac{|x_1|^2}{\sigma_s^2 + \sigma_n^2} \right)} \frac{\pi (\sigma_s^2 + \sigma_n^2)}{\exp \left(-\frac{|x_2|^2}{\sigma_s^2 + \sigma_n^2} \right)} \right) \\
&= c_1 + c_2 \sum_{k=\theta}^{\theta+L-1} \left(\operatorname{Re}\{e^{j2\pi\varepsilon} x_1 x_2^*\} - \rho (|x_1|^2 + |x_2|^2) \right) \\
&= c_1 + c_2 (|\gamma(\theta)| \cos(2\pi\varepsilon + \angle\gamma(\theta)) - \rho\mathcal{E}(\theta)),
\end{aligned}$$

where

$$\gamma(\theta) = \sum_{k=\theta}^{\theta+L-1} x_1 x_2^*, \quad (26)$$

$$\mathcal{E}(\theta) = \frac{1}{2} \sum_{k=\theta}^{\theta+L-1} (|x_1|^2 + |x_2|^2), \quad (27)$$

and c_1 and c_2 are complex constants, independent of θ and ε . Since the maximizing argument of $\Lambda(\theta, \varepsilon)$ is independent of the constants c_1 and c_2 , the ML-estimate $(\hat{\theta}_{\text{ML}}, \hat{\varepsilon}_{\text{ML}})$ also maximizes (10).

Averaging log-likelihood functions

Assume that the observation interval consists of $M(N + L) + N$ samples and that it contains M complete OFDM symbols. The arrival time θ is, as before, the index of the first sample of the first complete symbol, modelling the unknown channel delay. Consider the cyclic prefixes \mathcal{I}_m and their copies \mathcal{I}'_m for each symbol $m = 0, \dots, M - 1$:

$$\begin{aligned}
\mathcal{I}_m &\equiv \{m(N + L) + \theta, \dots, m(N + L) + \theta + L - 1\}, \\
\mathcal{I}'_m &\equiv \{m(N + L) + \theta + N, \dots, m(N + L) + \theta + N + L - 1\},
\end{aligned}$$

see Figure 9.

Define the union of all these indexes

$$\begin{aligned}
\mathcal{I} &\equiv \bigcup_{m=0}^{M-1} \mathcal{I}_m, \\
\mathcal{I}' &\equiv \bigcup_{m=0}^{M-1} \mathcal{I}'_m.
\end{aligned}$$

The observation samples $r(k)$, $k = 1, 2, \dots, M(N + L) + N$ can now be divided into the samples $r(k)$, $k \in \mathcal{I} \cup \mathcal{I}'$, which are pairwise dependent, and the remaining samples

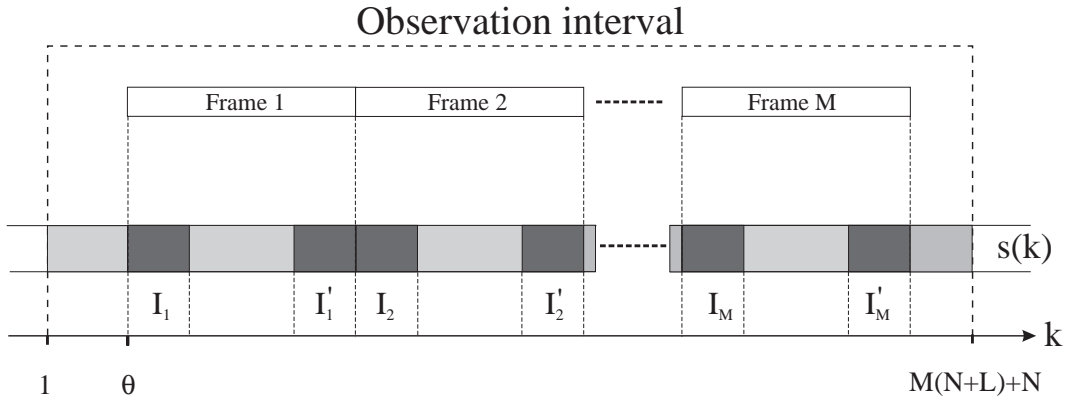


Figure 9: Observed signal $s(k)$ when averaging over several symbols.

$r(k)$, $k \notin \mathcal{I} \cup \mathcal{I}'$ which are independent. Using these properties, the probability density function of the observation can be written as

$$f(\mathbf{r}) = \prod_{k \in \mathcal{I}} f(r(k), r(k+N)) \prod_{k \notin \mathcal{I}} f(r(k)) = \prod_{k \in \mathcal{I}} \frac{f(r(k), r(k+N))}{f(r(k)) f(r(k+N))} \prod_k f(r(k)).$$

The last factor is independent of θ and ε and can thus be omitted. The remaining part can be rewritten due to the independence of samples from different symbols

$$\prod_{k \in \mathcal{I}} \frac{f(r(k), r(k+N))}{f(r(k)) f(r(k+N))} = \prod_{m=0}^{M-1} \left(\prod_{k \in \mathcal{I}_m} \frac{f(r(k), r(k+N))}{f(r(k)) f(r(k+N))} \right). \quad (28)$$

Since the innermost product is the likelihood function of symbol m , the likelihood function given the observation of M symbols is

$$\Lambda(\theta, \varepsilon) = \log f(\mathbf{r} | \theta, \varepsilon) = C + \sum_{m=0}^{M-1} \Lambda_m(\theta, \varepsilon), \quad (29)$$

where the constant C corresponds to the part that is independent of θ and ε .

References

- [1] John A. C. Bingham. Multicarrier modulation for data transmission: An idea whose time has come. *IEEE Communications Magazine*, 28(5):5–14, May 1990.
- [2] Radio broadcasting systems; Digital Audio Broadcasting (DAB) to mobile, portable and fixed receivers. ETS 300 401, ETSI – European Telecommunications Standards Institute, Valbonne, France, February 1995.
- [3] T. de Couasnon, R. Monnier, J.B. Rault, OFDM for Digital TV Broadcasting. *Signal Processing*, 39(1–2):1–32, September 1994.

- [4] Leonard J. Cimini. Analysis and simulation of a digital mobile channel using orthogonal frequency division multiplexing. *IEEE Trans. Comm.*, COM-33(7):665–675, July 1985.
- [5] P.S. Chow, J.C. Tu, and J.M. Cioffi. Performance evaluation of a multichannel transceiver system for ADSL and VHDSL services. *IEEE J. Sel. Areas Comm.*, 9(6):909–919, August 1991.
- [6] K Sistanizadeh, P.S. Chow, and J.M Cioffi. Multi-tone transmission for asymmetric digital subscriber lines(ADSL). In *Proc. Intern. Conf. Comm.*, pages 756–760. ICC '93, May 1993.
- [7] Lei Wei and Christian Schlegel. Synchronization requirements for multi-user OFDM on satellite mobile and two-path rayleigh fading channels. *IEEE Trans. Comm.*, 43(2/3/4):887–895, Feb/Mar/Apr 1995.
- [8] Thierry Pollet and Marc Moeneclaey. Synchronizability of OFDM signals. In *Proceedings of GLOBECOM'95*, volume 3, pages 2054–2058. IEEE, November 1995.
- [9] T. Pollet, M. van Bladel, and M. Moeneclaey. BER sensitivity of OFDM systems to carrier frequency offset and Wiener phase noise. *IEEE Trans. on Commun.*, 43(2/3/4):191–193, Feb/Mar/Apr 1995.
- [10] William D. Warner and Cyril Leung. OFDM/FM frame synchronization for mobile radio data communication. *IEEE Trans. Vehicular Tech.*, 42(3):302–313, August 1993.
- [11] P. J. Tourtier, R. Monnier, and P. Lopez. Multicarrier modem for digital HDTV terrestrial broadcasting. *Signal Processing: Image Communication*, 5(5–6):379–403, December 1993.
- [12] F. Daffara and A. Chouly. Maximum likelihood frequency detectors for orthogonal multicarrier systems. In *1993 IEEE International Conference on Communications*, pages 766–771. IEEE, May 1993.
- [13] Jan-Jaap van de Beek, Magnus Sandell, Mikael Isaksson, and Per Ola Börjesson. Low-complex frame synchronization in OFDM systems. In *Proc. of Intern. Conf. on Universal Personal Comm.*, pages 982–986. ICUPC '95, November 1995.
- [14] P.H. Moose. A technique for orthogonal frequency division multiplexing frequency offset correction. *IEEE Trans. Comm.*, 42(10):2908–2914, October 1994.
- [15] Flavio Daffara and Ottavio Adami. A new frequency detector for orthogonal multicarrier transmission techniques. In *Proc. VTC'95*, volume 2, pages 804–809, Chicago, Illinois, USA, July 1995. IEEE.
- [16] Magnus Sandell, Jan-Jaap van de Beek, and Per Ola Börjesson. Timing and frequency synchronization in OFDM systems using the cyclic prefix. In *1995 International Symposium on Synchronization*, pages 16–19, December 1995.

- [17] M. Alard and R. Lassalle. Principles of modulation and channel coding for digital broadcasting mobile receivers. *EBU Review – Technical*, (224):168–190, August 1987.
- [18] Jan-Olof Gustavsson and Per Ola Börjesson. A simultaneous maximum likelihood estimator based on a generalized matched filter. In *Proceedings of the 1994 IEEE international conference of acoustics, speech and signal processing (ICASSP'94)*, Adelaide, Australia, April 1994. IEEE.
- [19] G. C. Carter, Coherence and Time Delay Estimation. *Proc. of the IEEE*, 75(2):236–255, February 1987.
- [20] W. C. Jakes, *Microwave Mobile Communications*. Classic Reissue. IEEE Press, Piscataway, New Jersey, 1974.

Estimation of Synchronization Parameters

Jan-Jaap van de Beek

Luleå University of Technology
Division of Signal Processing
Luleå, Sweden

April 1996

Supervisor

Professor Per Ola Börjesson, Luleå University of Technology.

Abstract

This thesis deals with the estimation of synchronization parameters in Orthogonal Frequency Division Multiplexing (OFDM) communication systems and in active ultrasonic measuring systems. Estimation methods for the timing and frequency offset and for the attenuation taps of the frequency selective channel are presented and investigated.

In OFDM communication systems the estimation of the timing offset of the transmitted data frame is one important parameter. This offset provides the receiver with a means of synchronizing its sampling clock to that of the transmitter. A second important parameter is the offset in the carrier frequency used by the receiver to demodulate the received signal.

For OFDM systems using a cyclic prefix, the joint Maximum Likelihood (ML) estimation of the timing and carrier frequency offset is introduced. The redundancy introduced by the prefix is exploited optimally. This novel method is derived for a non-dispersive channel. Its performance, however, is also evaluated for a frequency-selective Rayleigh-fading radio channel. Time dispersion causes an irreducible error floor in this estimator's performance. This error floor is the limiting factor for the applicability of the timing estimator. Depending on the requirements, it may be used in either an acquisition or a tracking mode. For the frequency estimator the error floor is low enough to allow for stable frequency tracking.

A low-complex variant of the timing offset estimator is presented allowing a simple implementation. This is the ML estimator, given a 2-bit representation of the received signal as the sufficient statistics. Its performance is evaluated for a frequency-selective Rayleigh-fading radio channel and for a twisted-pair copper channel. Simulations show this estimator to have a similar error floor as the full resolution ML estimator.

The problem of estimating the propagation time of a signal is also of interest in active pulse echo systems, such as are used in, *e.g.*, radar, medical imaging, and geophysics. The Minimum Mean Squared Error (MMSE) estimator of arrival time is derived and investigated for an active airborne ultrasound measurement system. Besides performing better than the conventional *Maximum a Posteriori* (MAP) estimator, this method can be used to develop different estimators in situations where the system Signal to Noise Ratio (SNR) is unknown.

Coherent multi-amplitude OFDM receivers generally need to compensate for a frequency selective channel in order to detect transmitted data symbols reliably. For this purpose, a channel equalizer needs to be fed estimates of the subchannel attenuations.

The linear MMSE estimator of these attenuations is presented. Of all linear estimators, this estimator optimally makes use of the frequency correlation between the subchannel attenuations. Low-complex modified estimators are proposed and investigated. The proposed modifications cause an irreducible error floor for this estimator's performance, but simulations show that for SNR values up to 20 dB, the improvement of a modified estimator compared to the Least Squares (LS) estimator is at least 3 dB.

Publications

The following chronologically ordered publications represent the work I have carried out during the last three years. This thesis comprises an introduction, the original text of four of these publications ([1]–[3] and [5]), and a summary. These four publications (reformatted to suit the format of this thesis) are included in full. Results related to the work presented in [2] will be published as [6]. The main part of the work presented in [5] has been published as [4].

- [1] J.J. van de Beek, P.O. Börjesson, H. Ericsson, J-O. Gustavsson, L. Olsson, ‘MMSE Estimation of Arrival Time with Application to Ultrasonic Signals’, Research Report TULEA 1993:29, Division of Signal Processing, Luleå University of Technology, 1993. (**Part III**)
- [2] J.J. van de Beek, O. Edfors, M. Sandell, S.K. Wilson, P.O. Börjesson, ‘On Channel Estimation in OFDM Systems’, In *Proceedings of the 1995 IEEE 45th International Vehicular Technology Conference*, pp 815–819, Chicago, USA, 1995. (**Part IV**)
- [3] J.J. van de Beek, M. Sandell, M. Isaksson, P.O. Börjesson, ‘Low-Complex Frame Synchronization in OFDM Systems’, In *Proceedings of the 4th International Conference on Universal Personal Communications (ICUPC’95)*, pp 982–986, Tokyo, Japan, November 1995. (**Part II**)
- [4] M. Sandell, J.J. van de Beek, P.O. Börjesson, ‘Timing and Frequency Synchronization in OFDM Systems Using the Cyclic Prefix’, In *Proceedings of the 1995 International Symposium on Synchronization*, pp 16–19, Essen, Germany, December 1995.
- [5] J.J. van de Beek, M. Sandell, P.O. Börjesson, ‘ML Estimation of Timing and Frequency Offset in Multicarrier Systems’, Research Report TULEA 1996:09, Division of Signal Processing, Luleå University of Technology, 1996. (**Part I**)
- [6] O. Edfors, M. Sandell, J.J. van de Beek, S.K. Wilson, P.O. Börjesson, ‘OFDM Channel Estimation by Singular Value Decomposition’, To appear in *Proceedings of the 1996 IEEE 46th International Vehicular Technology Conference*, Atlanta, USA, 1996.

Contents

Abstract	v
Publications	vii
Acknowledgements	xi
Introduction: Synchronization Parameters and Signal Models	1
1 Introduction	3
2 Ultrasound Signal Model	4
3 OFDM Signal Models	6
4 Thesis Organization	8
I ML Estimation of Timing and Frequency Offset in Multicarrier Systems	13
1 Introduction	15
2 The OFDM system model	16
3 Maximum Likelihood estimation	19
4 Synchronization	21
5 Simulations	23
6 Discussion	26
The log-likelihood function	27
Averaging log-likelihood functions	28
II Low-Complex Frame Synchronization in OFDM Systems	33
1 Introduction	35
2 The OFDM Model	36
3 Synchronization Methods	37
4 Simulations	40
5 Conclusions	44
Appendix	44
III MMSE Estimation of Arrival Time with Application to Ultrasonic Signals	47
1 Introduction	49
2 Analysis	50
3 Error Bounds	51
4 Simulations & Experiments	53
5 Discussion	56

IV On Channel Estimation in OFDM Systems	63
1 Introduction	65
2 System Description	66
3 Channel Estimation	68
4 Simulations	70
5 Conclusions	73
Summary	77

Acknowledgements

This thesis presents a large part of the work I have carried out at the Division of Signal Processing, Luleå University of Technology, during the last three years. The four papers comprising it were written in a highly cooperative atmosphere and I want at this point to acknowledge a number of people.

About two and a half years ago, after I had worked some time in Luleå and Ronneby, I was invited to join the Division of Signal Processing in Luleå and continue my studies as a PhD student. My answer was by no means obvious. I want to thank my supervisor, Per Ola Börjesson, for making me accept the invitation. His enthusiasm, support, and encouragement were hard to resist, for which I am very grateful. I have never regretted my move and I look forward to the future.

Many former and present colleagues in Luleå have been of help. I want to emphasize the value and influence of our conversations and discussions in my work: perhaps their contribution to this thesis is less obvious, but it is very much appreciated.

I specially wish to mention Anders Grennberg and my coauthors Håkan Eriksson (now with Ericsson Mobile Communications AB), Lennart Olsson (now with Telia Research AB), Ove Edfors and Magnus Sandell. Of all the persons mentioned on this page (but for one), I undoubtedly spent most of my time in Luleå with Ove and Magnus. Not only has this time been challenging, stimulating and cooperative, it has also been (probably more importantly) a lot of fun.

I want to thank my coauthors Jan-Olov Gustavsson at the University College of Karlskrona/Ronneby, Mikael Isaksson at Telia Research AB, and Sarah Kate Wilson, at Purdue University. I also thank Paul Petersen for his efforts to make parts of this thesis readable and understandable.

Two more groups of people deserve notice on this page: the Department of Signal Processing, at the University College of Karlskrona/Ronneby, and the Communication Systems (Ksu) group at Telia Research AB. The existing arrangement by which the staff of Ksu cooperates with my colleagues and me is a fortunate circumstance, worth preserving and developing.

The work presented in this thesis was essentially carried out within the Center for Distance Spanning Technology (CDT) and within the Telecommunications Framework Program of the Swedish National Board for Industrial and Technical Development (NUTEK). I want to acknowledge CDT and NUTEK for their efforts and support.

Being a PhD student is quite an intense way of living. It involves some clear choices of priority in exchange for an enjoying and enriching time. Inevitably, the lives of my nearest are affected too. In this light, I finally thank my parents and my Mia for their comprehension, love, and support.

Luleå, Good Friday 1996.

Introduction: Synchronization Parameters and Signal Models

Introduction: Synchronization Parameters and Signal Models

J.J. van de Beek

Division of Signal Processing
Luleå University of Technology
S-971 87 Luleå, Sweden

1 Introduction

In a digital radio communication system, information symbols are transmitted by means of suitably chosen waveforms and symbol rate and modulated by a carrier signal with a suitably chosen frequency. Variable factors in the radio environment, however, may generate fluctuations in how these symbols are actually received. These fluctuations comprise alterations in the received signal's waveform (shape), symbol rate, and carrier frequency. Multipath propagation in combination with variable propagation times is the main cause of these fluctuations [9].

Because of these fluctuations, the receiver's knowledge of the symbol rate, the carrier frequency, and the constellation of transmitted waveforms is not always enough to assure reliable detection. In order to demodulate the received waveform coherently and to detect the information symbols properly, the receiver needs to counteract these channel uncertainties: it must be synchronized to the remote transmitter [9, 34].

Synchronization, as discussed in this thesis, covers all operations applied to the received signal to deal with channel uncertainties. Typically, in a coherent receiver, the receiver needs to regenerate a coherent replica of the carrier, generate a properly synchronized sample-clock, and counteract channel dispersion. We call these three operations, each of which compensates for some channel uncertainty, carrier-synchronization, symbol-synchronization and channel-synchronization. Channel synchronization is usually referred to as equalization.

Reliable communication over a time varying channel necessitates synchronization of the receiver. Depending on the data rate and the type of modulation, the demands on one or more of the synchronization tasks may be rather high. In order to perform these tasks adequately, the carrier phase, symbol timing, and channel dispersion must all be estimated and tracked by the receiver.

This thesis deals with the estimation of synchronization parameters in an *Orthogonal Frequency Division Multiplexing* (OFDM) system and in an active ultrasound measurement system. It is based on [1]–[6]. The actual synchronization process, *i.e.*, the estimate-aided compensation for the channel impairments, is beyond the scope of this thesis.

Figure 1 shows the discrete time model we adopt to illustrate the estimation problem. The transmitted signal $s(k)$ is transmitted over a time varying frequency selective channel and distorted by white Gaussian noise $n(k)$. In addition to this white Gaussian noise,

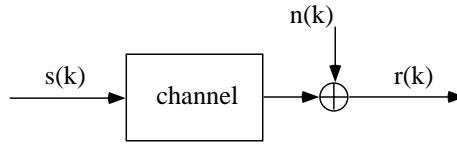


Figure 1: General system model.

the corruption of $s(k)$ will in this thesis be characterized by a few additional parameters: A delay, or timing offset θ , a frequency offset ε , and the frequency attenuation taps of the linear dispersive channel. These parameters are considered as synchronization parameters. Depending on the particular synchronization problem, the channel is modelled differently.

The estimation of these synchronization parameters may be interpreted as a measurement of the channel. In order to perform this measurement, the receiver must have some knowledge about the transmitted signal. In a digital communication system the receiver always has some *a priori* information. The finite waveform constellation and the data rate used by the transmitter are, for example, known. But there may be more information at hand. In particular, a known pilot signal may be transmitted periodically, entirely for channel measurement purposes.

When the communication system provides additional *a priori* knowledge about the transmitted signal, the receiver can better measure the channel characteristics. Channel measurement, however, only serves the purpose of making the transmission of information more efficient. Too much knowledge about the transmitted signal, although allowing for excellent channel measurement, may reduce the rate of information transmission and violate this higher purpose.

In the next sections we describe the parameter estimation problems in OFDM systems. The knowledge that the receiver has about the transmitted signal is explicitly formulated and the different channel models are introduced.

2 Ultrasound Signal Model

In this section, we start with a simple channel model. Of the parameters identified in the previous section only the timing uncertainty is taken into account.

In **Part 3** of this thesis we consider an active ultrasound measurement system. The purpose of this system is to measure the profile of 3-dimensional surfaces. An air-adapted focused ultrasonic transducer is used for the transmission of a short ultrasound pulse and for the reception of the reflected echo from the surface. Figure 2 shows a particular ultrasound echo from a surface perpendicular to the transducer. The pulse's propagation time θ is assumed to be proportional to the distance between the transducer and the surface. The system generates a relief picture of a surface structure by estimating this propagation time for different reflection points on the surface.

The transmitted pulse $s(k)$ is a known, bandlimited signal. We assume that the signal energy outside the observation interval is approximately zero. The propagation time θ is the value taken by an integer valued stochastic variable Θ with a known a

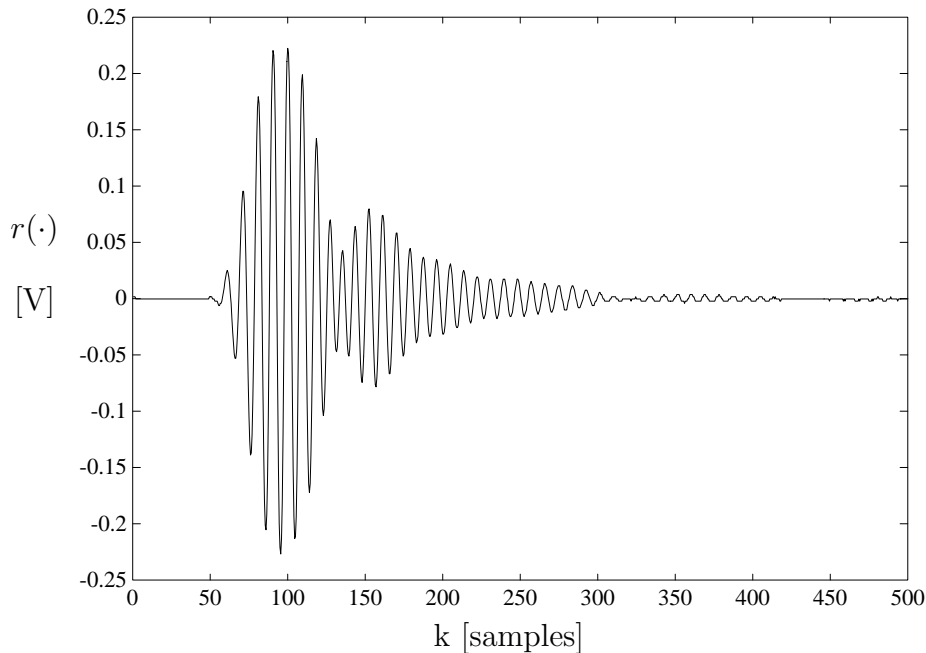


Figure 2: Received sample ultrasound echo from the ultrasonic system used.

priori probability density function $f_{\Theta}(\theta)$ having finite support and variance σ_{θ}^2 . If the transmitted signal is disturbed by additive white Gaussian noise, the received signal $r(k)$ is given by

$$r(k) = s(k - \theta) + n(k), \quad k = 0, \dots, N - 1. \quad (1)$$

This measuring system is shown in Figure 3. This model is a special case of the signal model as shown in Figure 1. The problem is to estimate the time delay θ from the observed samples $r(k)$.

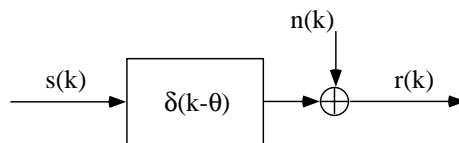


Figure 3: Ultrasound system model.

This problem and the signal model (1) describe many different measuring systems. It is used in, *e.g.*, sonar, radar, medical imaging, and geophysics. A lot of research has been done to understand and solve this problem, see for example [10, 11, 14, 21, 22, 23, 26, 28, 31, 36, 45]. Research related to the performance of the proposed estimators is reported in, for example, [12, 24, 27, 40, 41, 42, 46].

In the measuring system the synchronization parameter θ describes the distance to the surface of the measuring object. Unlike the transmitted signal in communication systems, the signal $s(k)$ is not used to carry information for communication purposes,

and the resulting estimates of θ are not fed back for compensation (synchronization) purposes. Rather, they are further processed to accurately present the surface structure.

3 OFDM Signal Models

In **Parts 1, 2, and 4** of this thesis we consider an OFDM communication system. The OFDM modulation technique has gained an increased interest during the last years. It has been adapted as the European standard for digital broadcast radio [7, 19] and is being studied for the use in broadcast television [16, 29, 37], and mobile personal communication systems [15]. Moreover, it has been proposed for digital subscriber lines [13, 35]. An OFDM system is modelled as shown in Figure 4.

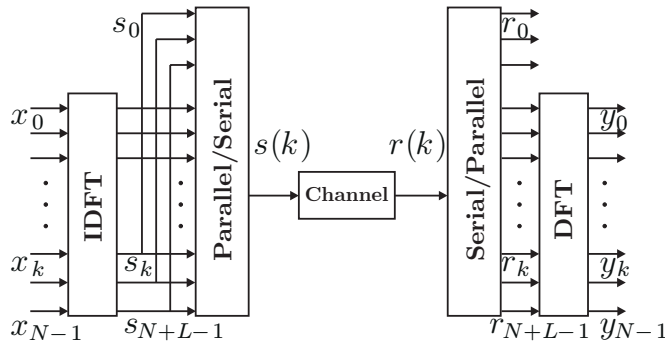


Figure 4: An OFDM system.

The complex data symbols x_k are modulated on N subcarriers by an inverse discrete Fourier transform (IDFT) and the last L samples are copied and put as a preamble (cyclic prefix) to form the OFDM symbol $[s_0 \dots s_{N+L-1}]$. This data vector is serially transmitted over a discrete-time channel, whose impulse response is shorter than L samples. At the receiver, the cyclic prefix is removed and the signal r_k is demodulated with a discrete Fourier transform (DFT).

The insertion of a cyclic prefix avoids ISI and preserves the orthogonality between the tones, resulting in the simple input-output relation [8]

$$y_k = h_k x_k + n_k, \quad k = 0, \dots, N-1, \quad (2)$$

where h_k is the complex valued channel attenuation at the k^{th} subcarrier and n_k is a sample from an additive complex white Gaussian noise process. In spite of the loss of transmission power and bandwidth associated with the cyclic prefix, the simple channel equalization for the multi-channel structure (2) generally motivates the use of the cyclic prefix [8]. An equivalent model of an OFDM system according to (2) is shown in Figure 5. The uncertainty in the dispersion by the channel thus shows up as a multiplicative distortion for each subcarrier. The estimation of the subchannel attenuations h_k has been examined in, *e.g.*, [25, 43, 44].

With the aid of pilot symbols, this problem is addressed in **Part 4** and the signal model (2) is adopted. The transmitted signal $s(k)$ now consists of complex, known data

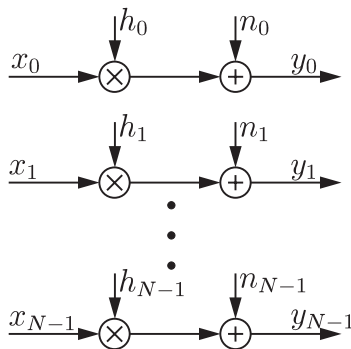


Figure 5: Equivalent OFDM system model.

symbols. Typically, the receiver transmits known OFDM symbols on a periodic basis, especially for channel measurement purposes. The N subchannel attenuations h_k are stochastic and correlated. The correlations between the attenuations can be exploited by a linear estimator, as described in **Part 4**.

The uncertainty in the arrival time of the OFDM symbol is modelled as a delay in the channel impulse response, *i.e.*, $\delta(k - \theta)$, where θ is the integer-valued unknown arrival time of a symbol. The uncertainty in carrier frequency due to a difference in the local oscillators in the transmitter and receiver gives rise to a shift in the frequency domain. Such behaviour is modelled as a complex multiplicative distortion of the received data, with a factor $e^{j2\pi\epsilon k/N}$, where ϵ denotes the difference in the frequency of the transmitter and receiver oscillators as a fraction of the inter-carrier spacing. Hence, the received signal is

$$r(k) = s(k - \theta)e^{j2\pi\epsilon k/N} + n(k). \quad (3)$$

This channel model is shown in Figure 6. This system model is also a special case of the signal model shown in Figure 1. The goal is to estimate θ and ϵ from the observation

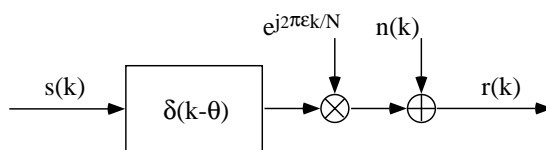


Figure 6: OFDM system model.

signal $r(k)$. Time and frequency synchronization problems in OFDM have been examined in, *e.g.*, [17, 18, 30, 32, 33, 38, 39]

In **Parts 1** and **2** of this thesis, the problem of estimating the time and frequency offset is addressed and the signal model (3) is adopted. The transmitted signal $s(k)$, which is a sum of weighted complex exponentials is modelled as a stochastic signal. It can be shown that $s(k)$ is close to a complex Gaussian process when the number of subchannels is large [20]. Due to the redundancy of the cyclic prefix, however, this Gaussian process is not white. The receiver, knowing the probability structure of $s(t)$, can exploit the correlation for the estimation of θ and ϵ .

4 Thesis Organization

This thesis comprises 4 parts that have been written independently and with a view to publish them as research reports, scientific articles, or conference proceedings. The organization of the individual parts, perhaps seeming repetitive in the context of this thesis, should be seen in this light. The problems, identified in this introductory chapter are discussed in detail in these parts. They are also followed by a summary of important results.

Part 1 describes the joint estimation of the timing and carrier frequency offset in OFDM systems. It has been published as a Research Report [5] and presented in part at the 1995 International Symposium on Synchronization, Essen, Germany [4]. How the timing offset estimator can be modified in order to achieve an estimator with low complexity is discussed in **Part 2**. These results were presented at the 4th International Conference on Universal Personal Communications, Tokyo, Japan (ICUPC'95) [3].

Part 3 describes the related problem of the estimation of the propagation time in an ultrasound measurement system. This has been published as a Research Report [1].

Finally, **Part 4** discusses the frequency correlation between channel attenuations in an OFDM system and methods to exploit this correlation in the channel estimator. It has been published at the 1995 IEEE 45th International Vehicular Technology Conference (VTC'95), Chicago, USA [2]. Related results will be published at the 1996 IEEE 46th International Vehicular Technology Conference (VTC'96), Atlanta, USA [6].

References

- [1] J.J. van de Beek, P.O. Börjesson, H. Ericsson, J-O. Gustavsson, L. Olsson, MMSE Estimation of Arrival Time with Application to Ultrasonic Signals, Research Report TULEA 1993:29, Division of Signal Processing, Luleå University of Technology.
- [2] J.J. van de Beek, O. Edfors, M. Sandell, S.K. Wilson, P.O. Börjesson, On Channel Estimation in OFDM Systems, In *Proceedings of the 1995 IEEE 45th International Vehicular Technology Conference*, pp 815–819, Chicago, USA, 1995.
- [3] J.J. van de Beek, M. Sandell, M. Isaksson, P.O. Börjesson, Low-Complex Frame Synchronization in OFDM Systems, In *Proceedings of the 4th International Conference on Universal Personal Communications (ICUPC'95)*, pp 982–986, Tokyo, Japan, November 1995.
- [4] M. Sandell, J.J. van de Beek, P.O. Börjesson, Timing and Frequency Synchronization in OFDM Systems Using the Cyclic Prefix, In *Proceedings of the 1995 International Symposium on Synchronization*, pp 16–19, Essen, Germany, December 1995.
- [5] J.J. van de Beek, M. Sandell, P.O. Börjesson, ML Estimation of Timing and Frequency Offset in Multicarrier Systems, Research Report TULEA 1996:09, Division of Signal Processing, Luleå University of Technology.

- [6] O. Edfors, M. Sandell, J.J. van de Beek, S.K. Wilson, P.O. Börjesson, OFDM Channel Estimation by Singular Value Decomposition, To appear in *Proceedings of the 1996 IEEE 46th International Vehicular Technology Conference*, Atlanta, USA, 1996.
- [7] M. Alard and R. Lassalle. Principles of modulation and channel coding for digital broadcasting mobile receivers. *EBU Review – Technical*, (224):168–190, August 1987.
- [8] J.A.C. Bingham. Multicarrier modulation for data transmission: An idea whose time has come. *IEEE Communications Magazine*, 28(5):5–14, May 1990.
- [9] R.E. Blahut, *Digital Transmission of Information*. Addison-Wesley, 1990.
- [10] J.N. Bradley and R. L. Kirlin. Delay estimation by expected value. *IEEE Transactions on acoustics, speech and signal processing*, 32(1):19–27, 1984.
- [11] G.C. Carter, Coherence and Time Delay Estimation. *Proc. of the IEEE*, 75(2):236–255, February 1987.
- [12] D. Chazan, M. Zakai, and J. Ziv. Improved lower bounds on signal parameter estimation. *IEEE Transactions on information theory*, 21:90–93, 1975.
- [13] P.S. Chow, J.C. Tu, and J.M. Cioffi. Performance evaluation of a multichannel transceiver system for ADSL and VHDSL services. *IEEE J. Sel. Areas Comm.*, 9(6):909–919, August 1991.
- [14] S.K. Chow and P.M. Schultheiss. Delay estimation using narrow band processes. *IEEE Transactions on acoustics, speech and signal processing*, 29(3):478–484, 1981.
- [15] L.J. Cimini. Analysis and simulation of a digital mobile channel using orthogonal frequency division multiplexing. *IEEE Trans. Comm.*, COM-33(7):665–675, July 1985.
- [16] T. de Couasnon, R. Monnier, J.B. Rault, OFDM for Digital TV Broadcasting. *Signal Processing*, 39(1–2):1–32, September 1994.
- [17] F. Daffara and O. Adami. A new frequency detector for orthogonal multicarrier transmission techniques. In *Proc. VTC'95*, volume 2, pages 804–809, Chicago, Illinois, USA, July 1995. IEEE.
- [18] F. Daffara and A. Chouly. Maximum likelihood frequency detectors for orthogonal multicarrier systems. In *1993 IEEE International Conference on Communications*, pages 766–771. IEEE, May 1993.
- [19] Radio broadcasting systems; Digital Audio Broadcasting (DAB) to mobile, portable and fixed receivers. ETS 300 401, ETSI – European Telecommunications Standards Institute, Valbonne, France, February 1995.

- [20] R. Gross and D. Veeneman, Clipping Distortion in DMT ADSL Systems, *Electron. Lett.*, Vol. 29, no. 24, pp. 2080–2081, November 1993.
- [21] J-O. Gustavsson and P.O. Börjesson. ‘Ankomsttidsskattning av rektangulära pulser i en klass av icke-normalfördelat brus’. In B. O. Rönnang, editor, *Proceedings of RVK 90*, pages 282–288, Chalmers Institute of Technology, Sweden, April 1990. ‘Svenska nationalkommitten for radiovetenskap’.
- [22] J-O. Gustavsson and P.O. Börjesson. A generalized matched filter. In *Proceedings of the third international symposium on signal processing and its applications*, pages 16–22, Gold coast, Australia, August 1992.
- [23] J.C. Hassab and R.E. Boucher. Optimum estimation of time delay by a generalized correlator. *IEEE Transactions on acoustics, speech and signal processing*, 27(4):373–380, 1979.
- [24] J.C. Hassab and R.E. Boucher. Performance of the generalized cross correlator in the presence of a strong spectral peak in the signal. *IEEE Transactions on acoustics, speech and signal processing*, 29(3):549–555, 1981.
- [25] P. Hoeher, TCM on frequency-selective land-mobile fading channels, In *Proc. of the 5th Tirrenia International Workshop on Digital Communications*, Tirrenia, Italy, September 1991.
- [26] J.P. Ianniello. Time delay estimation via cross-correlation in the presence of large estimation errors. *IEEE Transactions on acoustics, speech and signal processing*, 30(6):998–1003, 1982.
- [27] K.L. Kosbar. A lower bound for the error-variance of maximum-likelihood delay estimates of discontinuous pulse waveforms. *IEEE Transactions on information theory*, 38(2):451–457, 1992.
- [28] C.H. Knapp and G.C. Carter. The generalized correlation method for estimation of time delay. *IEEE Transactions on acoustics, speech and signal processing*, 24(4):320–327, 1976.
- [29] B. Marti et al., European activities on digital television broadcasting—from company to cooperative projects, *EBU Technical Review*, no. 256, pp. 20–29, 1993.
- [30] P.H. Moose. A technique for orthogonal frequency division multiplexing frequency offset correction. *IEEE Trans. Comm.*, 42(10):2908–2914, October 1994.
- [31] N.J. Nilsson. On the optimum range resolution of radar signals in noise. *IRE transactions on information theory*, pages 245–253, October 1961.
- [32] T. Pollet and M. Moeneclaey. Synchronizability of OFDM signals. In *Proceedings of GLOBECOM’95*, volume 3, pages 2054–2058. IEEE, November 1995.

- [33] T. Pollet, M. van Bladel, and M. Moeneclaey. BER sensitivity of OFDM systems to carrier frequency offset and Wiener phase noise. *IEEE Trans. on Commun.*, 43(2/3/4):191–193, Feb/Mar/Apr 1995.
- [34] J.G. Proakis, Digital Communications. McGraw-Hill, 1995.
- [35] K. Sistanizadeh, P.S. Chow, and J.M. Cioffi. Multi-tone transmission for asymmetric digital subscriber lines(ADSL). In *Proc. Intern. Conf. Comm.*, pages 756–760. ICC '93, May 1993.
- [36] N. Sundström, P.O. Börjesson, N-G. Holmer, L. Olsson, and H.W. Persson, Registration of surface structures using airborne focused ultrasound. *Ultrasound in medicine and biology*, 17(5):513–518, 1991.
- [37] P.J. Tourtier, R. Monnier, and P. Lopez. Multicarrier modem for digital HDTV terrestrial broadcasting. *Signal Processing: Image Communication*, 5(5–6):379–403, December 1993.
- [38] W.D. Warner and C. Leung. OFDM/FM frame synchronization for mobile radio data communication. *IEEE Trans. Vehicular Tech.*, 42(3):302–313, August 1993.
- [39] L. Wei and C. Schlegel. Synchronization requirements for multi-user OFDM on satellite mobile and two-path rayleigh fading channels. *IEEE Trans. Comm.*, 43(2/3/4):887–895, Feb/Mar/Apr 1995.
- [40] A.J. Weiss. Composite bounds on arrival time estimation errors. *IEEE Transactions on areospace and electronic systems*, 22(6):751–756, 1986.
- [41] A.J. Weiss and E. Weinstein. A lower bound on the mean-square error in random parameter estimation. *IEEE Transactions on information theory*, 31(5):680–682, 1985.
- [42] A.J. Weiss and E. Weinstein. Fundamental limitations in passive time delay estimation – Part 1: Narrowband systems. *IEEE Transactions on acoustics, speech and signal processing*, 31(2):472–486, 1983.
- [43] S.K. Wilson, Digital Audio Broadcasting in a Fading and Dispersive Channel, PhD-thesis, Stanford University, August 1994.
- [44] S.K. Wilson, R.E. Khayata and J.M. Cioffi, 16-QAM modulation with orthogonal frequency-division multiplexing in a Rayleigh-fading environment, In *Proc. VTC-1994*, pp. 1660–1664, Stockholm, Sweden, June 1994.
- [45] A. Zeira and P. M. Schultheiss, Thresholds and related problems in time delay estimation. In *Proceedings of international conference on acoustics, speech and signal processing*, pages 1261–1264, Toronto, Canada, May 1991. IEEE.
- [46] J. Ziv and M. Zakai. Some lower bounds on signal parameter estimation. *IEEE Transactions on information theory*, 15(3):386–391, 1969.

Part II

Low-Complex Frame Synchronization in OFDM Systems

This part has been published as

J.J. van de Beek, M. Sandell, M. Isaksson, P.O. Börjesson, 'Low-Complex Frame Synchronization in OFDM Systems', In *Proceedings of the 4th International Conference on Universal Personal Communications (ICUPC'95)*, pp 982–986, Tokyo, Japan, November 1995.

Low-Complex Frame Synchronization in OFDM Systems

J.J. van de Beek¹ M. Sandell¹ M. Isaksson²
P.O. Börjesson¹

¹ Div. of Signal Processing
Luleå University of Technology
S-971 87 Luleå, Sweden

² Telia Research AB
S-977 75 Luleå, Sweden

Abstract – In this paper a novel data-based frame synchronization method for OFDM-systems is presented. OFDM frames are shown to contain sufficient information to synchronize a system without the use of pilots. The cyclic extension, preceding OFDM frames, is of decisive importance for this method. Based on only the sign bits of the in-phase and the quadrature components of the received OFDM signal, the maximum likelihood solution is derived. This solution basically consists of a correlator, a moving sum and a peak detector. The stability of the generated frame-clock is improved significantly by averaging over a few number of frames. Simulations show that this low-complex, averaging method can be used to synchronize an OFDM system on twisted pair copper wires and in slowly fading radio channels.

1 Introduction

Orthogonal frequency-division multiplexing (OFDM) systems have gained an increased interest during the last years [1]. Their use in wireless applications such as digital broadcast radio [2] and television [3], as well as mobile communication systems [4], is currently investigated.

By the name of *discrete multitone* (DMT) modulation, OFDM is also examined for broadband digital communication on the existing copper network. The OFDM technique has been proposed both for *high bit-rate digital subscriber lines* (HDSL) and *asymmetric digital subscriber lines* (ADSL) [5, 6].

A problem in the design of OFDM receivers and receivers for block transmission systems in general, is the unknown time instant to start sampling a new frame. Such a frame clock may be generated with the aid of pilot symbols known to the receiver [7]. The structure of the transmitted OFDM signal, however, offers the opportunity to generate a frame clock that works without the aid of such pilots.

In this paper we present and evaluate a novel method of synchronizing frames in OFDM systems. Two key elements will rule the entire discussion. The first element is the idea that the data itself contains sufficient information to perform satisfactory synchronization. This concept is also discussed in [8], and, for the estimation of a frequency offset, in [9]. The frame synchronization methods we present exploit the cyclic extension preceding the symbol frames, commonly accepted as a means to mitigate *inter-symbol*

interference (ISI) in OFDM systems [1, 2]. The use of pilots is thus avoided. The second element is the demand that the methods must be low-complex and hence attractive to implement. We present methods, that only use the in-phase and quadrature sign bits of the OFDM data.

In Section 2, the OFDM transmission model is described. The synchronization problem is formulated, and optimal solutions are presented in Section 3. Finally, in Section 4, simulation results are given for transmission over typical copper wire channels and slowly fading radio channels.

2 The OFDM Model

Consider the transmission of complex numbers x_k , taken from some signal constellation (e.g., PSK, QAM). Fig. 1 illustrates the discrete-time OFDM system model we will use in the sequel. The data x_k are modulated on N subcarriers by an *inverse discrete Fourier transform* (IDFT) and the last L samples are copied and put as a preamble (cyclic prefix) to form the OFDM frame s_k .

The channel impulse response $h(k)$ is, for now, assumed to affect the signal $s(k)$ only by complex, additive white Gaussian noise (AWGN), $n(k)$, *i.e.*, $h(k) = \delta(k)$. In Section 4 we consider other channel impulse responses. Thus, the received signal, $r(k)$, is given by

$$r(k) = s(k) + n(k). \quad (1)$$

The data y_k are obtained by discarding the first L samples (cyclic prefix) of $r(k)$ and demodulating the N remaining samples of each frame by means of a DFT.

The structure of the transmitted signal $s(k)$ is illustrated in Fig. 2. We assume that the data x_k constitute a white process. Further, if the number of subcarriers is sufficiently large, then $s(k)$ is approximately a complex Gaussian process, whose real and imaginary parts are independent [10]. This process, however, is not white, since the appearance of a cyclic extension yields a non-zero correlation between pairs of samples, part of the cyclic extension, spaced N samples apart. Thus, $r(k)$ is not a white process either. On the contrary, $r(k)$ contains information about when a new frame starts by its probabilistic structure. This is the crucial observation that offers the opportunity for frame synchronization based on $r(k)$. In the next section, this idea is formally shaped and elaborated.

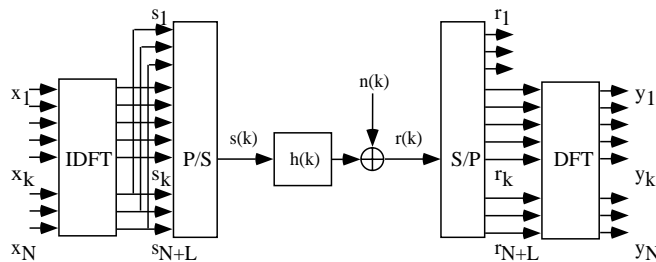


Figure 1: OFDM system.

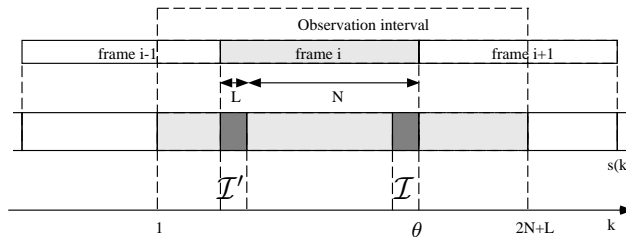


Figure 2: Structure of OFDM signal with cyclicly extended frames, $s(k)$.

3 Synchronization Methods

3.1 Optimal Synchronization

Assume that we observe $2N + L$ consecutive samples of $r(k)$, *cf.* Fig. 2, and that these samples contain one complete $(N + L)$ -sample OFDM frame. Notice that the other N samples in this observation interval are independent.

The position of this frame within the observed block of samples, however, is unknown. Define the integer time instant θ as the time index of the last sample of this frame, and the index sets $\mathcal{I} \triangleq [\theta - L + 1, \theta]$ and $\mathcal{I}' \triangleq [\theta - N - L + 1, \theta - N]$, see Fig. 2. The set \mathcal{I} thus contains the indices of the data samples that are copied into the cyclic prefix, and the set \mathcal{I}' contains the indices of this prefix.

In [11] it is shown that the log-likelihood function for the time instant θ given the observations $r(k)$, $k = 1, \dots, 2N + L$ is

$$\begin{aligned} \Lambda_{\text{r}}(\theta) &= & (2) \\ &= \sum_{k=\theta-L+1}^{\theta} 2(1-\rho)\text{Re}\{r(k)r^*(k-N)\} - \rho \cdot |r(k) - r(k-N)|^2 \end{aligned}$$

where

$$\rho = \frac{E\{|s(k)|^2\}}{E\{|s(k)|^2\} + E\{|n(k)|^2\}} = \frac{\text{SNR}}{\text{SNR} + 1} \quad (3)$$

is the correlation coefficient of a sample $r(k)$, $k \in \mathcal{I}$ and the sample $r(k-N)$ in the cyclic prefix. The signal-to-noise ratio (SNR) is defined as $E\{|s(k)|^2\}/E\{|n(k)|^2\}$.

The *maximum likelihood* (ML) estimation of θ given $r(k)$, $\hat{\theta}_r$, is the argument maximizing (2). Thus, depending on SNR, the correlation and the squared difference between received data samples spaced N samples apart are weighted in an optimal way, the correlation term positively and the squared difference term negatively. This estimate, $\hat{\theta}_r$, whose implementation may be complex, will be used as a reference in Section 4.

3.2 Low-Complex Synchronization

In the discussion that follows, we will comply with the objective that the synchronization must be low-complex, and we quantize the in-phase and quadrature components of $r(k)$

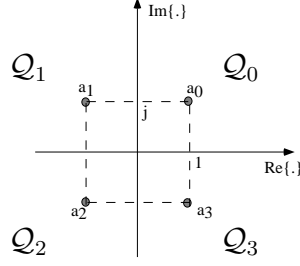


Figure 3: Geometric representation of the signal set \mathcal{A} and the quadrants $\mathcal{Q}_i, i = 0, 1, 2, 3$ of the complex plane.

to form the complex sequence $c(k) = Q[r(k)], k = 1, \dots, 2N + L$ where $Q[\cdot]$ denotes the complex quantizer

$$Q[x] \triangleq \text{sign}(\text{Re}\{x\}) + j\text{sign}(\text{Im}\{x\}), \quad (4)$$

$$\text{sign}(x) \triangleq \begin{cases} +1, & x \geq 0, \\ -1, & x < 0. \end{cases} \quad (5)$$

The signal $c(k)$ is a complex bitstream, *i.e.*, $c(k)$ can only take one of four different values in the alphabet

$$\mathcal{A} = \{a_0, a_1, a_2, a_3\}, \{1 + j, -1 + j, -1 - j, 1 - j\}, \quad (6)$$

see Fig. 3. The sequence $c(k)$ can thus be represented by 2 bits, one for its real and one for its imaginary part. In spite of this quantization, $c(k)$ still contains information about θ . A sample $c(k), k \in \mathcal{I}$, is correlated with $c(k - N)$, while all samples $c(k), k \notin \mathcal{I} \cup \mathcal{I}'$, are independent.

The probability for all $2N + L$ samples of $c(k)$ to be observed simultaneously, given a certain value of θ , can be separated in the marginal probabilities for its samples to be observed, except for those samples $c(k), k \in \mathcal{I} \cup \mathcal{I}'$, which are pairwise correlated. Denote the joint probability density function for $c(k)$ and $c(k - N), k \in \mathcal{I}$, by $p_1(\cdot)$, and the probability density function for $c(k), k \notin \mathcal{I} \cup \mathcal{I}'$, by $p_2(\cdot)$. Then, the log-likelihood function of θ given $c(k)$ becomes

$$\Lambda_{\mathcal{C}}(\theta) = \log p_{\theta}(c) = \log \left\{ \prod_{k \in \mathcal{I}} p_1(c(k), c(k - N)) \cdot \prod_{k \notin \mathcal{I} \cup \mathcal{I}'} p_2(c(k)) \right\}. \quad (7)$$

The ML estimator of θ given $c(k)$, $\hat{\theta}_{\mathcal{C}}$, maximizes this function with respect to θ . For $k \notin \mathcal{I} \cup \mathcal{I}'$, $p_2(c(k)) = \frac{1}{4}$, since $r(k)$ is a zero-mean complex Gaussian process with independent real and imaginary parts. Hence, the second product in the maximization of (7) is a constant, which can be omitted. The ML estimate $\hat{\theta}_{\mathcal{C}}$ becomes

$$\begin{aligned} \hat{\theta}_{\mathcal{C}} &= \arg \max_{\theta} \Lambda_{\mathcal{C}}(\theta) \\ &= \arg \max_{\theta} \sum_{k \in \mathcal{I}} \log p_1(c(k), c(k - N)) \end{aligned}$$

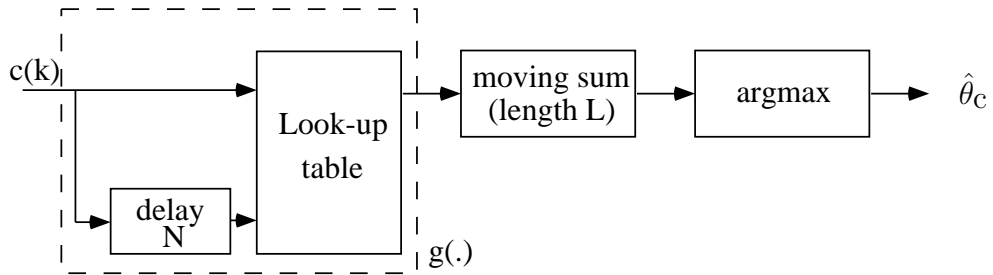


Figure 4: Look-up table implementation of the ML estimator.

$$\begin{aligned}
 &= \arg \max_{\theta} \sum_{k=\theta-L+1}^{\theta} \log p_1(c(k), c(k-N)) \\
 &= \arg \max_{\theta} (g * h)(\theta),
 \end{aligned} \tag{8}$$

where

$$g(k) = \log p_1(c(k), c(k-N)), \tag{9}$$

$$h(k) = \begin{cases} 1, & 0 \leq k < L-1, \\ 0, & \text{otherwise,} \end{cases} \tag{10}$$

and $*$ denotes convolution. To obtain the log-likelihood function we thus feed the sequence $c(k)$ through a nonlinearity $g(\cdot)$ and process the resulting sequence by means of a moving sum of length L , see Fig. 4. The ML estimation of θ selects the peaks of this function.

Fig. 4 suggests that the OFDM signal can be processed continuously. The sequence out of the moving sum is a concatenation of log-likelihood functions $\Lambda_c(\theta)$ for consecutive OFDM frames. In Fig. 5 such a sequence is shown.

In the appendix, the ML estimator based on $c(k)$ is determined by calculating the probability density $p_1(\cdot)$. Moreover, it is shown that taking the real part of the correlation between $c(k)$ and $c(k-N)$, instead of applying the non-linearity $g(k)$ yields an equivalent and attractive structure for the ML estimator, as illustrated in Figure 6. The estimate $\hat{\theta}_c$ feeds a *phase-locked loop* (PLL) in order to generate a frame clock.

3.3 Averaging the Log-Likelihood Function

In most applications the arrival time θ is approximately constant over several, say M , received frames. This essentially means that instead of just one frame $r(k)$, M frames are observed simultaneously containing information about the unknown θ . Generalizing the discussion preceding (7), it can be shown that the log-likelihood function for θ given $c_i(k), i=1, \dots, M$ becomes

$$\Lambda_a(\theta) \sim \sum_{i=1}^M \Lambda_c^i(\theta) \tag{11}$$

where $\Lambda_c^i(\theta)$ represents the log-likelihood function (7) of θ given frame $c_i(k)$. The ML estimate $\hat{\theta}_a$ given $c_i(k), i=1, \dots, M$, is the argument maximizing (11).

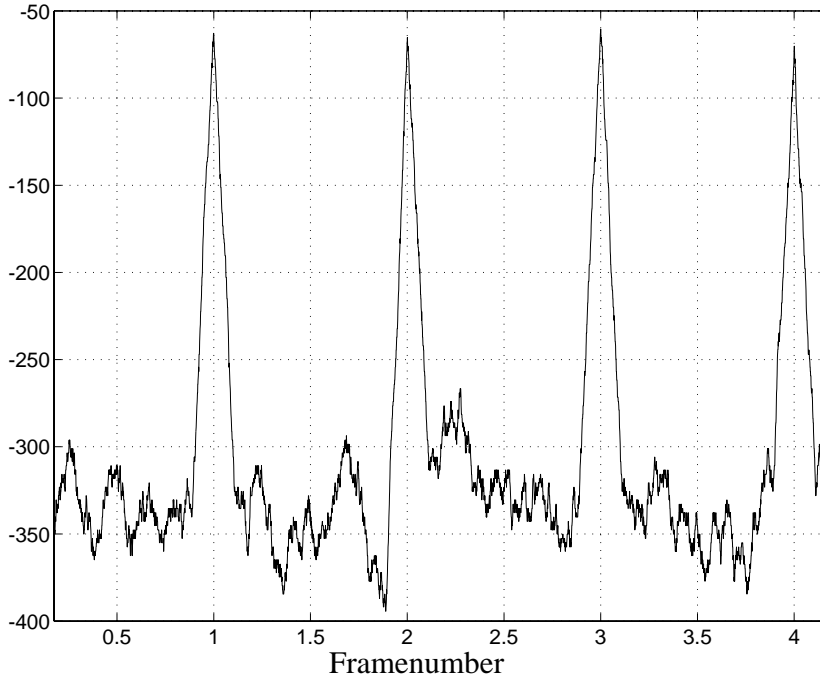


Figure 5: Concatenated log-likelihood functions whose peaks generate estimates of θ . SNR=15 dB.

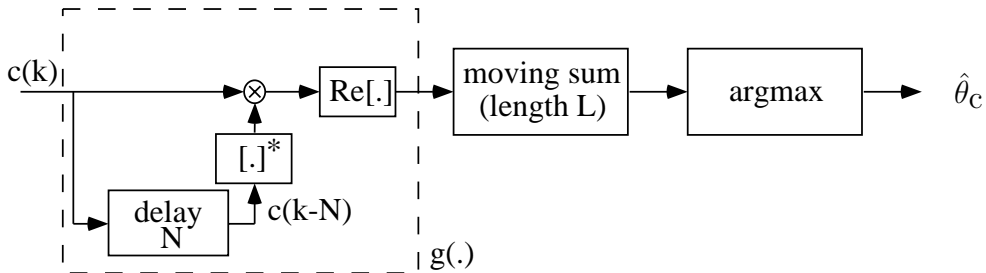


Figure 6: Equivalent implementation of the ML estimator.

4 Simulations

We have performed Monte Carlo simulations to evaluate the performances of the suggested synchronization algorithms. First, the estimator performance for the AWGN channel is presented. Furthermore, two possible channel environments for OFDM, static and fading, are simulated. These environments both suffer from time dispersion, which makes the definition of the arrival time θ a delicate matter. In some sense, this arrival time and the influence of the channel on the data are interchangeable. In the following we will define the arrival time θ as the center of energy of the channel impulse response. We evaluate the performance of the estimator using the variance of the estimation error $E\{(\hat{\theta} - \theta)^2\}$.

Moreover, fading radio channels introduce a time-variant arrival time. This arrival

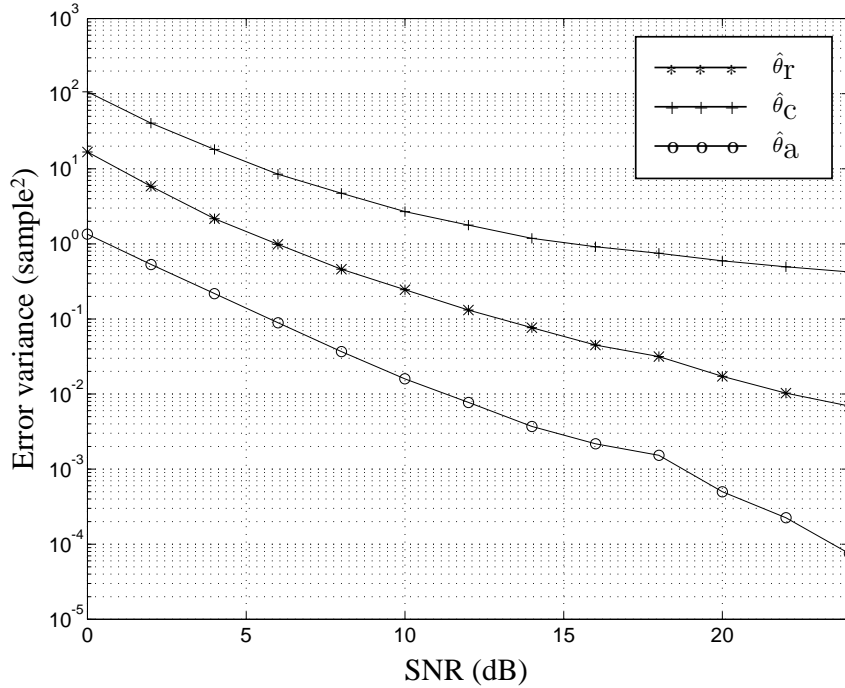


Figure 7: Error variance for AWGN channel of three estimators: The ML estimator, $\hat{\theta}_r$, based on $r(k)$; the ML estimator, $\hat{\theta}_c$, based on the quantized data $c(k)$; and the averaging estimator, $\hat{\theta}_a$.

time varies depending on the relative Doppler. This readily limits the usefulness of the averaging estimator. We present simulations of a slowly fading radio channel, allowing for moderate averaging.

4.1 AWGN Channel

An OFDM system consisting of 1024 subcarriers and a guardspace of 128 samples, *i.e.*, 1/8 of the frame length is considered. White, complex Gaussian noise is added and the error variance as a function of SNR is estimated. For each SNR value, 10,000 frames are simulated. Estimation error variance curves for the estimators $\hat{\theta}_c$ and $\hat{\theta}_a$, *i.e.*, the arguments maximizing (7) and (11), respectively, are compared to the ML estimator $\hat{\theta}_r$ that works on the unquantized OFDM-signal (2).

The simulations indicate that the estimators are approximately unbiased and the error variances $E\{(\hat{\theta} - \theta)^2\}$ are shown in Fig. 7. For practical channel environments, the assumption of infinite bandwidth is not realistic. The curves in Fig. 7 illustrate the performance of the derived estimators under ideal conditions. Notice the relative performances of the estimators. The estimator performance is degraded by regarding only the sign bits in the received signal $r(k)$. However, by averaging over only 8 consecutive frames before peak detection, the estimator performance is improved by a factor that is

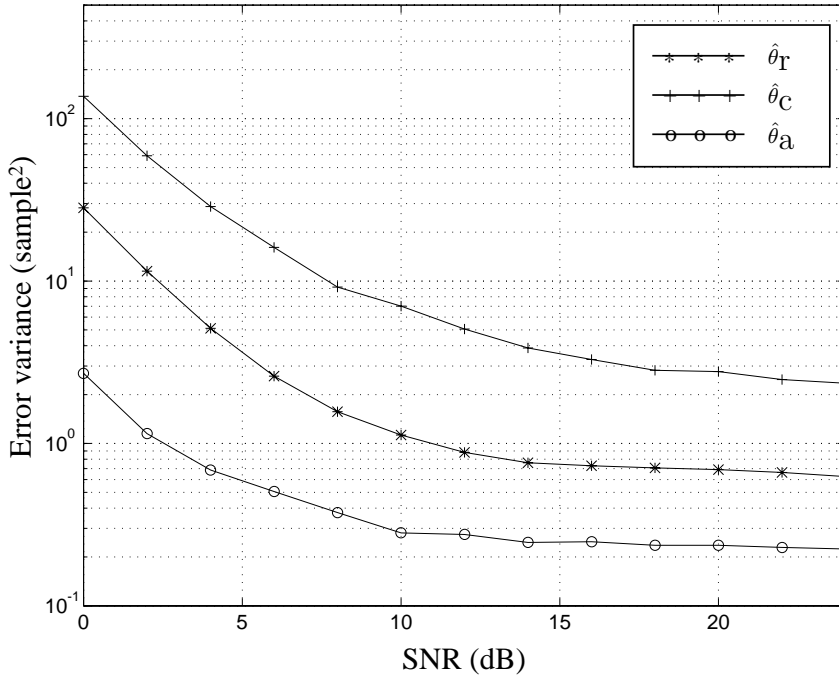


Figure 8: Error variance for twisted pair channel of three estimators: The ML estimator, $\hat{\theta}_r$, based on $r(k)$; the ML estimator, $\hat{\theta}_c$, based on the quantized data $c(k)$; and the averaging estimator, $\hat{\theta}_a$.

significantly larger than 64 (the improvement of averaging the estimates after the peak detection).

4.2 Twisted Pair Channel

A broadband OFDM system for HDSL with the following specifications is simulated. The impulse response of the channel, which is normalized to have unit energy, is obtained from measurements by Telia Research AB on a 503 meter copper wire and has a duration of approximately $2 \mu\text{s}$. The sample frequency is 12.5 MHz, and the guardspace has a length of 128 samples, *i.e.*, $10.24 \mu\text{s}$. The system uses 1024 subcarriers. Noise with a power spectral density proportional to $f^{3/2}$ is added to simulate near-end crosstalk (NEXT) [5, 12]. The SNR in this case is defined as before, *i.e.* the quotient between signal and noise power at the receiver and again 10,000 frames are simulated for each SNR value.

The error variances are shown in Fig. 8. The estimators behave in approximately the same way as they do in a AWGN channel environment. The error variance, however, has increased, due to the channel impulse response of the copper wire, which bounds the error variance. Notice that the estimators are derived under the assumption that $c(k)$ are independent for $k \notin \mathcal{I} \cup \mathcal{I}'$. This assumption is violated as a consequence of the channel

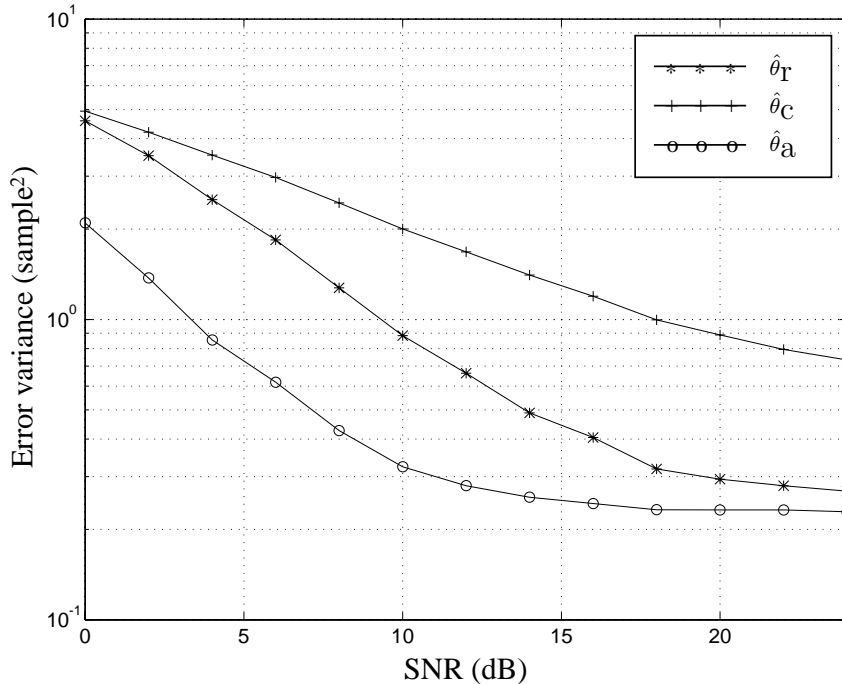


Figure 9: Error variance for fading radio channel of three estimators: The ML estimator, $\hat{\theta}_r$, based on $r(k)$; the ML estimator, $\hat{\theta}_c$, based on the quantized data $c(k)$; and the averaging estimator, $\hat{\theta}_a$.

impulse response. However, the error variance of the estimator $\hat{\theta}_a$ is still small and may be used to feed a PLL.

4.3 Fading Radio Channel

Finally, we evaluate a slowly fading channel environment. A wireless system operating at 2 GHz with a bandwidth of 5 MHz is simulated. In these simulations, an OFDM frame consists of 64 subcarriers with an additional 5 sample guardspace. A fading environment with additive white Gaussian noise and large-room characteristics is chosen: the channel impulse response has a maximum length of $0.35 \mu\text{s}$ [13], corresponding to 2 samples. The channel impulse response is modelled to consist of two independent Rayleigh-fading taps with equal average power. The mobile is assumed to be moving at a maximum speed of 5 km/h resulting in a maximum Doppler frequency of 10 Hz. This Doppler frequency is low enough to motivate the averaging of 8 frames in the synchronization algorithm, since the channel impulse response does not change significantly during this interval. In this simulation, 300,000 frames are used for each SNR value.

The same effects as in the copper wire experiments can be observed from Fig. 9, *i.e.*, the proportions of the error variances resemble each other, but the absolute values have increased. Again, the channel bounds the error variance and the curves level out at

ca. 15 dB. An increase of SNR beyond this threshold does not improve the estimators significantly.

5 Conclusions

In this paper we have shown how the cyclic extension of OFDM frames can be used to generate a frame clock at the receiver. The ML estimator $\hat{\theta}_T$, based on the received data, though optimal, may not be appropriate for use in practical systems, due to its complexity. The ML estimation based on only the sign bits of the data is given for the AWGN channel model and an averaging over several OFDM frames is proposed. Simulations suggest that this averaging significantly improves synchronization performance. For practical systems on copper wires and slowly fading channels the error variance of $\hat{\theta}_C$ is significantly improved. It can be used to feed a PLL, generating the system frame clock.

Appendix

Notice first that

$$c(k) = Q[r(k)] = a_l \Leftrightarrow r(k) \in \mathcal{Q}_l \quad (12)$$

where $\mathcal{Q}_l, l=0, 1, 2, 3$ are the quadrants of the complex plane as depicted in Fig. 3. Since the real and imaginary part of $r(k)$ are independent, we can write the probability

$$\Pr(r(k) \in \mathcal{Q}_l) = \Pr(\text{Re}\{r(k)\} \in \mathcal{H}_l) \Pr(\text{Im}\{r(k)\} \in \mathcal{H}'_l) \quad (13)$$

(see Fig. 3), where \mathcal{H}_l and \mathcal{H}'_l are the half-planes

$$\mathcal{H}_l = \begin{cases} \mathbb{R}^+, & l = 0, 3 \\ \mathbb{R}^-, & l = 1, 2 \end{cases}, \quad \mathcal{H}'_l = \begin{cases} \mathbb{R}^+, & l = 0, 1 \\ \mathbb{R}^-, & l = 2, 3 \end{cases}. \quad (14)$$

The joint probability $p_1(\cdot)$ in (7) can be written as

$$\begin{aligned} \Pr(c(k) = a_l, c(k-N) = a_n) &= \\ \Pr(r(k) \in \mathcal{Q}_l, r(k-N) \in \mathcal{Q}_n) &= \\ \Pr(\text{Re}\{r(k)\} \in \mathcal{H}_l, \text{Re}\{r(k-N)\} \in \mathcal{H}_n) &\times \\ \Pr(\text{Im}\{r(k)\} \in \mathcal{H}'_l, \text{Im}\{r(k-N)\} \in \mathcal{H}'_n). & \end{aligned} \quad (15)$$

By applying the symmetry expressions for two real, zero-mean, jointly Gaussian variables x and y with correlation coefficient ρ , [14, pp. 137-138],

$$P^+ \triangleq \Pr((x, y) \in \mathbb{R}^+ \times \mathbb{R}^+) = \Pr((x, y) \in \mathbb{R}^- \times \mathbb{R}^-) \quad (16)$$

$$P^- \triangleq \Pr((x, y) \in \mathbb{R}^- \times \mathbb{R}^+) = \Pr((x, y) \in \mathbb{R}^+ \times \mathbb{R}^-),$$

the look-up table in Fig. 4 becomes

$c(k-N)$	a_0	a_1	a_2	a_3
$c(k)$				
a_0	$\log P^+P^+$	$\log P^-P^+$	$\log P^-P^-$	$\log P^+P^-$
a_1	$\log P^+P^-$	$\log P^+P^+$	$\log P^-P^+$	$\log P^-P^-$
a_2	$\log P^-P^-$	$\log P^+P^-$	$\log P^+P^+$	$\log P^-P^+$
a_3	$\log P^-P^+$	$\log P^-P^-$	$\log P^+P^-$	$\log P^+P^+$

The ML estimate (8) that uses this look-up table is not affected by an affine scaling $f(x) = ax+b, (a>0)$ of the values in the table, since it is a convex mapping. If we choose

$$f(x) = \frac{x - \log P^+P^-}{\log P^+P^+ - \log P^+P^-} \quad (17)$$

the non-linearity $f[g(l, n)]$ becomes

$c(k-N)$	a_0	a_1	a_2	a_3
$c(k)$				
a_0	1	0	-1	0
a_1	0	1	0	-1
a_2	-1	0	1	0
a_3	0	-1	0	1

Since

$$\text{Entry}(a_n, a_l) = \frac{1}{2} \text{Re}\{a_n a_l^*\}, \quad (18)$$

the look-up table may be implemented by taking the real part of $c(k)c^*(k-N)$.

References

- [1] J.A.C. Bingham, "Multicarrier modulation for data transmission: an idea whose time has come", *IEEE Communications Magazine*, Vol. 28, no. 5, pp. 5–14, May 1990.
- [2] M. Alard and R. Lassalle, "Principles of modulation and channel coding for digital broadcasting for mobile receivers", *EBU Review*, no. 224, pp. 3–25, August 1987.
- [3] B. Marti et al., "European activities on digital television broadcasting—from company to cooperative projects", *EBU Technical Review*, no. 256, pp. 20–29, 1993.
- [4] L.J. Cimini, Jr., "Analysis and Simulation of a Digital Mobile Channel using Orthogonal Frequency Division Multiplexing", *IEEE Trans. Comm.*, Vol. COM-33, no. 7, pp. 665–675, July 1985.
- [5] P.S. Chow, J.C. Tu, and J.M. Cioffi, "Performance evaluation of a Multichannel Transceiver System for ADSL and VHDSL Services", *IEEE J. Sel. Areas Comm.*, Vol. 9, no. 6, pp. 909–919, August 1991.

- [6] K. Sistanizadeh, P.S. Chow and J.M. Cioffi, “Multi-Tone Transmission for Asymmetric Digital Subscriber Lines (ADSL)”, *Proc. Intern. Conf. Comm.*, ICC '93, pp. 756–760, May 1993.
- [7] W.D. Warner and C. Leung, “OFDM/FM Frame Synchronization for Mobile Radio Data Communication”, *IEEE Trans. Veh. Techn.*, Vol. 42, no. 3, pp. 302–313, August 1993.
- [8] P.J. Tourtier, R. Monnier and P. Lopez, “Multicarrier modem for HDTV terrestrial broadcasting”, *Signal Processing: Image Communication*, Vol. 5, no. 5-6, pp. 379–403, December 1993.
- [9] F. Daffara and O. Adami, “A new frequency detector for orthogonal multicarrier transmission techniques”, In *Proc. VTC-95*, pp. 804–809, July 1995.
- [10] R. Gross and D. Veeneman, “Clipping Distortion in DMT ADSL Systems”, *Electron. Lett.*, Vol. 29, no. 24, pp. 2080–2081, November 1993.
- [11] M. Sandell, J.J. van de Beek, M. Isaksson, P.O. Börjesson, “Maximum Likelihood Synchronization in OFDM systems”, To appear as a Research Report, Div. of Signal Processing, Luleå University, Sweden.
- [12] J.-J. Werner, “The HDSL environment”, *IEEE J. Sel. Areas Comm.*, Vol. SAC-9, no. 6, pp. 785–800, August 1991.
- [13] U. Dersch and E. Zollinger, “Propagation Mechanism in Microcell and Indoor Environments”, *Proc. 4th Intern. Symp. on Personal, Indoor and Mobile Radio Comm.*, PIMRC '93, Yokohama, Japan, pp. 191, September 1993.
- [14] A. Papoulis, *Probability, Random Variables, and Stochastic Processes*, 2nd edition, McGraw-Hill, Inc., 1984

Part III

MMSE Estimation of Arrival Time with Application to Ultrasonic Signals

This part has been published as

J.J. van de Beek, P.O. Börjesson, H. Ericsson, J-O. Gustavsson, L. Olsson, 'MMSE Estimation of Arrival Time with Application to Ultrasonic Signals', *Research Report TULEA 1993:29*, Division of Signal Processing, Luleå University of Technology.

H. Ericsson is now with Ericsson Mobile Communications AB, Lund, Sweden.

MMSE Estimation of Arrival Time with Application to Ultrasonic Signals

J.J. van de Beek^{1,2} P.O. Börjesson¹ H. Eriksson^{1,2}
 J-O. Gustavsson^{1,2} L. Olsson¹

¹ Div. of Signal Processing
 Luleå University of Technology
 S-971 87 Luleå, Sweden

² Dept. of Signal Processing
 University College of
 Karlskrona/Ronneby
 372 25 Ronneby, Sweden

Abstract - This paper deals with arrival time estimation of a narrow-band signal disturbed by white gaussian noise. In order to estimate the distance between a transmitting source and a reflecting target an estimator, based on the criterion of minimum mean square error (MMSE), is investigated. The MMSE-estimator is implemented in an experimental ultrasound pulse-echo system, and results of comparative simulations between the MAP-estimator and the MMSE-estimator are given. The results are compared to the theoretical Weiss-Weinstein lower bound. As expected, the MMSE-estimator has smaller mean square error than the MAP-estimator. For high SNRs, however, the mean square error obtained by the MAP-estimator manages to approach that of the MMSE-estimator. Other differences between the two estimators are revealed in additional experiments in which the range estimates are used to generate 3-dimensional surface pictures.

1 Introduction

In various medical as well as seismic applications, man-made acoustic pulse-echo systems can be of great value. Many of these applications require the time interval between the transmission of a sound pulse and the reception of the corresponding echo to be estimated accurately.

A well-known method for the estimation of arrival time is the correlation method [1, 2, 3]. If the received echo is disturbed by white gaussian noise, the correlation method turns out to be a Maximum a Posteriori (MAP) estimator [4].

In many applications a strong sinusoidal component is present in the transmitted signal, and, since this sinusoid will also turn up in the correlator output, the MAP-estimator will encounter problems in selecting the peak corresponding to the time delay. The effect of a strong spectral peak in the signal on the estimator performance has been recognized and examined in e.g. [5, 6]. Although this peak ambiguity problem is rather an intrinsic feature of non-linear estimation than a property of the MAP-estimator, the question arises whether other estimation methods could better cope with this. In [7], this problem is treated by using an estimation method based on the criterion of minimum mean square error (MMSE). Although the presented results were promising, to our knowledge not much attention has been paid to the MMSE-estimation method since [8, 9, 10].

In this paper the MMSE-estimator of arrival time is reconsidered. A thorough derivation of the MMSE-estimator of the arrival time of a deterministic signal disturbed by zero mean, white gaussian noise is given and implementation problems are solved in chapter 2. In chapter 3 the Cramér-Rao and the Weiss-Weinstein lower bounds on the mean square error of arrival time estimates are summarized. In chapter 4 an implementation of an ultrasound system is described. In order to compare the MAP- and the MMSE-estimators, results from Monte Carlo simulations are presented and compared with the Weiss-Weinstein lower bound. Moreover, 3-dimensional ultrasonic pictures generated using the arrival time estimators are shown.

2 Analysis

The received signal $r(\cdot)$ is mathematically modelled by

$$r(k) = s(k - \theta) + n(k), \quad k = 0, \dots, N - 1 \quad (1)$$

where $s(\cdot)$ is the transmitted signal, $n(\cdot)$ is the disturbing noise and θ is the time delay to be estimated.

Assume that $s(\cdot)$ is a known, bandlimited signal and that $n(\cdot)$ is a realization of a stationary, zero mean, white gaussian random process with variance σ^2 . Furthermore, assume that the time delay θ is the value taken by a continuously valued stochastic variable Θ with a known a priori probability density function, $f_{\Theta}(\theta)$, having finite support and the variance σ_{θ}^2 .

From (1) it follows that $r(k)$ is the value taken by a stochastic variable $R(k)$, for every k . In the following R denotes the N -dimensional stochastic variable $[R(0), R(1), \dots, R(N - 1)]$, while r is the value taken by this variable.

A measure of an estimator's performance is $E[|\Theta - \hat{\theta}(R)|^2]$, where $\hat{\theta}(R)$ is an estimator of θ . The function $\hat{\theta}(r)$ minimizing this quantity, and henceforth referred to as the MMSE-estimator of θ , is obtained by calculating [4]

$$\hat{\theta}_{\text{MMSE}}(r) = E[\Theta | R = r]. \quad (2)$$

In the following an expression for this expectation is derived, cf. [7] where a slightly different derivation is given. Since we deal with zero mean white gaussian noise, the conditional probability density function of $R(k)$ given $\Theta = \theta$ will be gaussian too, with mean value $s(k - \theta)$ and variance σ^2 . Hence, for the conditional probability density function $p_{R|\Theta}(r|\theta)$,

$$p_{R|\Theta}(r|\theta) = (\sqrt{2\pi\sigma^2})^{-N} e^{-\frac{1}{2\sigma^2} \sum (r(k) - s(k - \theta))^2}, \quad (3)$$

where the sum is taken over all sample values ($k = 0, \dots, N - 1$). Expanding the square, using Baye's rule and expression (3), it follows that the conditional probability density function $f_{\Theta|R}(\theta|r)$ is

$$f_{\Theta|R}(\theta|r) = \frac{1}{K} \cdot f_{\Theta}(\theta) e^{\frac{1}{\sigma^2} C(\theta)} \quad (4)$$

where

$$C(\theta) = \sum_{k=0}^{N-1} r(k)s(k-\theta) + \frac{1}{2}\epsilon(\theta), \quad (5)$$

K is a normalizing constant and $\epsilon(\theta)$ is a function of θ which can only assume very small values¹. The last expression is approximately the correlator output. The value of θ corresponding to the maximum of (4) provides the MAP-estimate of the time delay [4]. Using expression (4), (2) becomes

$$\begin{aligned} \hat{\theta}_{\text{MMSE}} &= \int \theta f_{\Theta|R}(\theta|r) d\theta \\ &= \frac{1}{K} \int \theta f_{\Theta}(\theta) e^{\frac{1}{\sigma^2}C(\theta)} d\theta. \end{aligned} \quad (6)$$

Since $\int f_{\Theta|R}(\theta|r) d\theta = 1$, the constant K becomes $K = \int e^{\frac{1}{\sigma^2}C(\theta)} f_{\Theta}(\theta) d\theta$, and (6) can now be written as

$$\hat{\theta}_{\text{MMSE}} = \frac{\int \theta e^{\frac{1}{\sigma^2}C(\theta)} f_{\Theta}(\theta) d\theta}{\int e^{\frac{1}{\sigma^2}C(\theta)} f_{\Theta}(\theta) d\theta}. \quad (7)$$

This expression is the basic appearance of the MMSE-estimator of arrival time. Implementing this form of the estimator may require the hardware to be able to deal with large numbers. In particular when the noise variance σ^2 is small, the exponent in (7) may be too large for accurate estimates to be calculated. For most SNRs, the value of $\frac{1}{\sigma^2}C(\theta)$ can still be handled. In order to address this numerical problem, (7) can be rewritten as

$$\hat{\theta}_{\text{MMSE}} = \frac{\int \theta e^{\frac{1}{\sigma^2}[C(\theta)-p]} f_{\Theta}(\theta) d\theta}{\int e^{\frac{1}{\sigma^2}[C(\theta)-p]} f_{\Theta}(\theta) d\theta}, \quad (8)$$

where $p = \max_{\theta} \{C(\theta)\} - M_0\sigma^2$, and where M_0 is chosen to match the hardware capabilities.

Notice that the estimation can be interpreted as a weighted average of the exponential function values. Notice further that the variance of the corrupting noise must be known or estimated before applying expression (7). It is therefore convenient to make a distinction between the true noise variance σ^2 and the variance used to design the MMSE-estimator, σ_D^2 . The influence of the choice of σ_D^2 on the performance of the MMSE-estimator will be discussed in chapter 4.

3 Error Bounds

An experimental comparison of the estimation error of the MMSE- and the MAP-estimators provides insight in the relative performance of the two methods. However,

¹ It is presupposed that θ and N can only assume values where $\epsilon(\theta) = \sum_{k \notin [0, N-1]} s^2(k-\theta) \approx 0$. That

is, the signal energy outside the observation interval, $\epsilon(\theta)$, is approximately zero, or equivalently, for all θ almost the whole signal energy is inside the observation interval.

some additional insight in the estimator performance can be gained by comparing the experimental mean square estimation error $\sigma_{\hat{\theta}}^2$ to theoretical bounds as the Cramér-Rao Lower Bound (CRLB) or the Weiss-Weinstein Lower Bound (WWLB).

Define the signal to noise ratio (SNR) as

$$\text{SNR} = \frac{E}{\sigma^2}, \quad E = \int s^2(t)dt = \int |S(f)|^2 df, \quad (9)$$

where $S(f)$ is the fourier transform of the signal $s(\cdot)$ and E is the signal energy. Provided that certain regularity conditions are fulfilled, the CRLB can be written as [4, 11]

$$\sigma_{\hat{\theta}}^2 \geq \frac{1}{4\pi^2 \bar{f}^2 \text{SNR} + A/\sigma^2}, \quad (10)$$

where A is a constant depending on the shape of $f_{\Theta}(\theta)$ but independent of $\sigma_{\hat{\theta}}^2$ and $E\{\theta\}$, $(\bar{f}^2)^{1/2}$ denotes the Gabor-bandwidth (or the rms-bandwidth) of the signal $s(\cdot)$ and is defined as

$$\bar{f}^2 = \frac{\int f^2 |S(f)|^2 df}{\int |S(f)|^2 df}. \quad (11)$$

The CRLB does not take into account the well-known threshold effect of time delay estimators, emphatically present in narrowband systems [12, 13, 14]. For SNR-values below a certain threshold the mean square error increases rapidly as the SNR decreases. When the bandwidth of the transmitted signal becomes narrower, this property becomes more pronounced. The SNR-region where the mean square error exceeds the CRLB, mainly due to the peak ambiguity error, is known as the peak ambiguous region. Several bounds incorporating this feature have been developed [14, 15, 16, 17, 18]. In chapter 4 the simulation results will be compared with the WWLB presented in [17, 18]. This bound applies explicitly to deterministic signals, it is easy to calculate, and assumes a uniform a priori distribution of Θ .

By assuming that Θ is uniformly distributed between 0 and D the WWLB can be written as [18]

$$\sigma_{\hat{\theta}}^2 \geq \max_{0 \leq h \leq D} J(h), \quad (12)$$

where

$$J(h) = \begin{cases} \frac{\frac{1}{2}h^2(1-\frac{h}{D})^2 e^{-\frac{\text{SNR}}{2}[1-\rho(h)]}}{1-\frac{h}{D}-(1-\frac{2h}{D})e^{-\frac{\text{SNR}}{4}[1-\rho(2h)]}}, & 0 \leq h < \frac{D}{2} \\ \frac{1}{2}h^2(1-\frac{h}{D})e^{-\frac{\text{SNR}}{2}[1-\rho(h)]}, & \frac{D}{2} \leq h < D \end{cases} \quad (13)$$

and where $\rho(\cdot)$ denotes the normalized autocorrelation function of the transmitted signal $s(\cdot)$.

The WWLB provides a tight lower bound on time delay estimates for a wide range of signal to noise ratios [18]. The WWLB takes into account the phenomenon of peak ambiguity. Notice that, except for the SNR, the WWLB only depends on the values of the signal autocorrelation function and on the a priori interval length.

4 Simulations & Experiments

This chapter provides performance results obtained by simulations and by using the experimental ultrasonic system described in detail in [19]. The system characteristics answer to those of a narrowband system, thus yielding the problem of detecting the correct peak of the correlation function at low SNRs.

An air-adapted focused ultrasonic transducer, designed by Persson for the purpose of the investigation presented in [19], with a centre frequency of 1 MHz and a focal distance of 45 mm is used for the transmission of a short ultrasound pulse and for the reception of the reflected echo. The echoes received are sampled with a sampling frequency of 10 MHz. Figure 1 shows a particular ultrasound echo from a surface perpendicular to the transducer. A sample conditional probability density function of Θ given $R = r$ is shown in figure 2. In the experiments the time delay Θ is assumed to have a uniform a priori distribution over the interval $[0, D]$. The MMSE-estimator can be calculated by (8) with the integrals taken over the a priori interval of Θ , thus accounting for the probability density function $f_{\Theta}(\theta)$. The MMSE-estimator is approximated by

$$\hat{\theta}_{\text{MMSE}} = \frac{\sum_{k=0}^{D/T_s} T_s k e^{\frac{1}{\sigma_D^2}[C(T_s k) - p]}}{\sum_{k=0}^{D/T_s} e^{\frac{1}{\sigma_D^2}[C(T_s k) - p]}} \quad (14)$$

with T_s as a step length and σ_D^2 , the design variance, as described in chapter 2. In order to speed up the calculation of the $\hat{\theta}_{\text{MMSE}}$, consider the function

$$Z(x) = \begin{cases} 0 & , e^{\frac{1}{\sigma_D^2}[C(x) - p]} < M_1 \\ e^{\frac{1}{\sigma_D^2}[C(x) - p]} & , e^{\frac{1}{\sigma_D^2}[C(x) - p]} \geq M_1. \end{cases} \quad (15)$$

The delay estimate is now calculated by replacing the exponential terms in (14) by the function $Z(T_s k)$. The value of M_1 is chosen to take only the significant terms in the sums of (14) into account. The exponential expression in (15) is evaluated considerably faster by choosing $M_2 = p + \sigma_D^2 \log M_1$ and comparing the correlator output with M_2 .

In the simulations a Monte Carlo technique is used to estimate the mean square error for a range of noise levels. The a priori density of Θ is chosen to be uniform between 0 and 255 samples, the parameter $M_1 = 0$ and the step length $T_s = \frac{1}{55}$. In these simulations the echo from a point on the surface of a piece of perspex is chosen to be the transmitted signal $s(\cdot)$ in (1), shown in figure 1. This signal is then randomly shifted in time with an artificial delay according to the a priori density of Θ , and subsequently disturbed by zero mean, white gaussian noise in order to obtain a specific SNR-level. The MMSE-estimator is adapted to each particular noise level by adjusting the value of σ_D^2 , i.e. $\sigma_D^2 = \sigma^2$.

Figure 3 shows the results of the simulations as well as the WWLB. The right hand side of (10) assuming that $f_{\Theta}(\theta)$ is such that A is finite and σ_{θ}^2 is infinite is also shown in the figure, i.e. the CRLB with no a priori information about Θ . As expected, the MMSE-estimator shows a smaller mean square error than the MAP-estimator over the

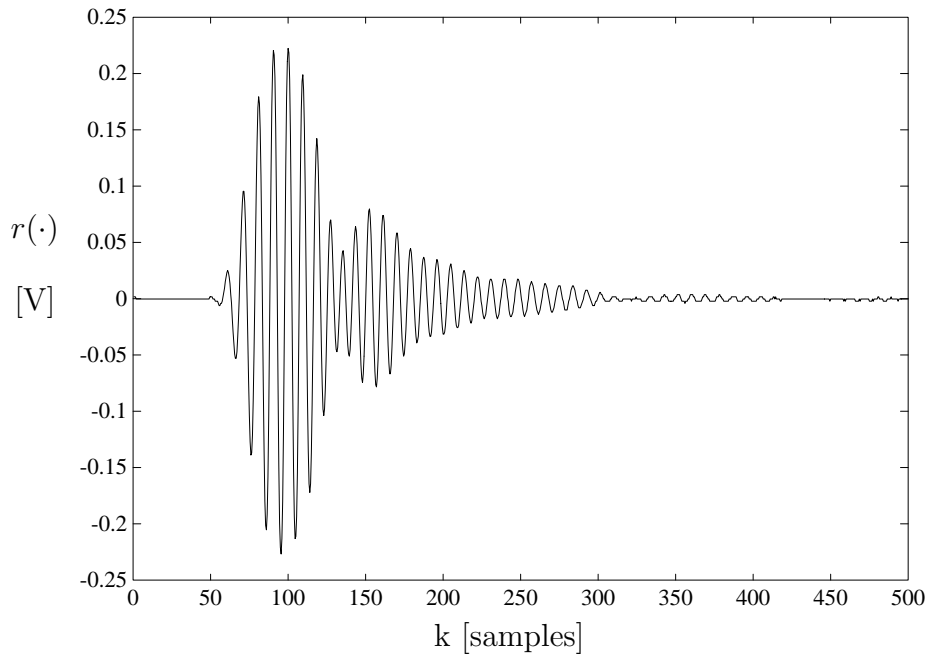


Figure 1: Received sample ultrasound echo from the ultrasonic system used.

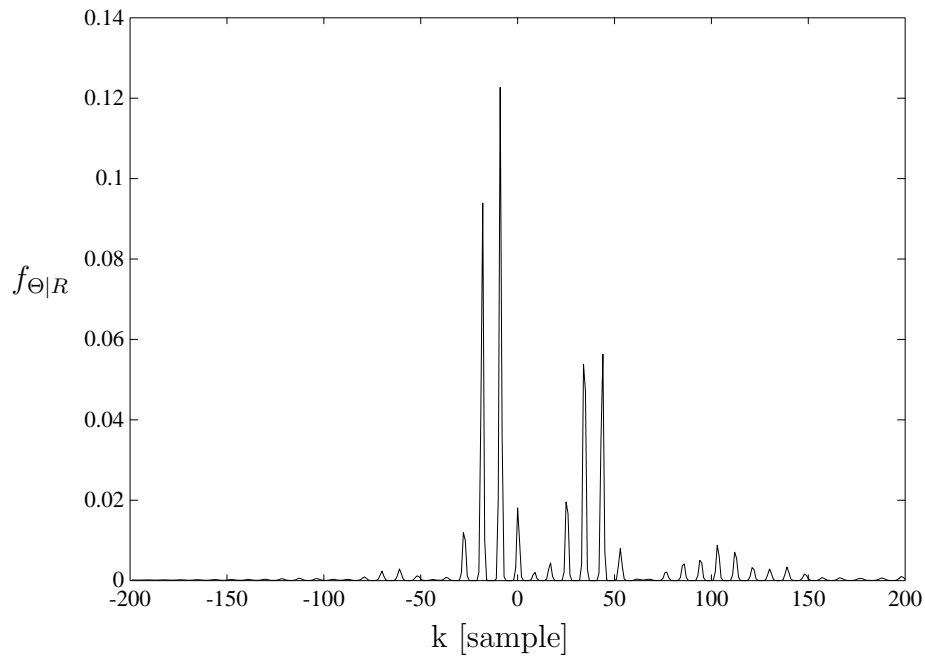


Figure 2: Sample density function for SNR = 10 dB.

$$\hat{E}\{(\hat{\theta}(R) - \theta)^2\}$$

(sample)²

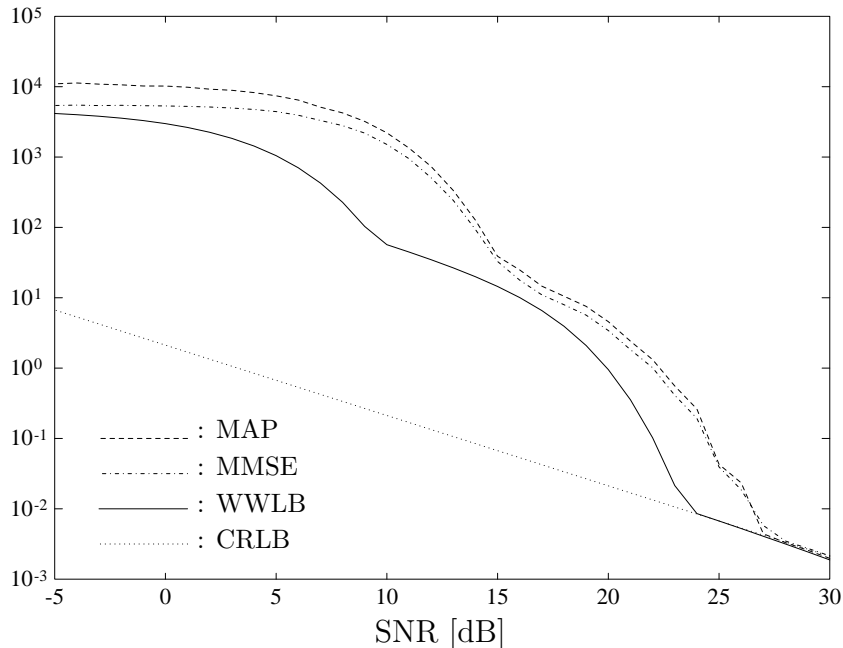


Figure 3: The sample mean square error of $\hat{\theta}$ plotted versus SNR, based on 10,000 simulations, together with the lower bounds presented in chapter 3.

entire range of SNRs. For high SNRs the mean square error of the MAP- estimator converges to the results of the implemented MMSE- estimator, since only the peak value of the correlator output (5) remains in the calculation of the MMSE-estimate after the modifications given in (14)–(15).

In the case of an extremely high noise level the received signal cannot be recovered anymore and the MMSE-estimate is set to the a priori mean delay. The threshold effect, appearing at moderate SNR can be observed readily. An examination of the correlator output for different SNRs shows that the signal under consideration causes two regions of peak ambiguity. For SNRs between approximately 15 dB and 25 dB, the ambiguity error is caused only by the two peaks adjacent to the peak corresponding to the true arrival time. Below approximately 15 dB SNR other peaks become ambiguous as well, and a second threshold occurs. The Weiss-Weinstein lower bound readily predicts this behaviour. Notice that in [18] a similar stepwise curve is derived for a trapezoidal pulse.

In order to gain insight in the practical differences between the MMSE- and MAP- estimators experiments have been carried out using the above mentioned equipment and the MMSE-estimator of (14) and by using (15). The observation interval is sufficiently long to contain the received signal², and the a priori density of Θ is chosen to be uniform between 0 and 255 samples, which corresponds to a distance span of approximately 4 mm.

The ultrasound system is used to generate a relief picture of a surface structure by estimating the arrival time of echoes from different surface points. In figure 4–7

²See footnote 1 on page 51

surface pictures of a Swedish five-crown coin are shown, obtained by the MMSE arrival time estimator for four different values of σ_D^2 in (14). Figure 8 shows the corresponding picture obtained with the MAP-estimator. Each picture is obtained by scanning the coin surface in 100 by 100 points with a distance of 0.3 mm between adjacent points. The sampling frequency is 10 MHz and the value of σ_D^2 in (14) is kept constant for all surface points.

The interpretation of the experimental results is a difficult problem. Still some valuable observations can be made and typical effects can be observed:

1. For small design variances, σ_D^2 , the resolution of the surface picture approaches that of the picture produced by the MAP-estimator. In accordance with the simulations when the true noise variance is low figure 4 and figure 8 are almost identical.
2. For σ_D^2 large, the generated surface picture is smoothed by the estimator. The estimator assumes a high noise level, while the received echoes are hardly disturbed by noise. Arrival times corresponding to neighbouring peaks of the correlator output will be considered as having a relatively high a posteriori probability of occurrence.
3. Deformations of the pulse shape turn out to be an important feature. Although a high axial resolution can be obtained, some limitations of the model under consideration are visible. The deformations of the pulshape and a reduced amount of energy are often found in reflections from regions on the coin where the coin does not have a plane and perpendicular surface. Such surfaces are e.g. slopes, edges and unevennesses, and the effects of this can be observed e.g. in fig 7 as the deep grooves. The model in (1) seems to lose its validity. By interpreting the change of the signal shape as coloured noise in (1), choosing a larger design variance σ_D^2 may be motivated.
4. Although figure 7 seems to be a bad reproduction of the real coin, there are details of the coin that are visible only in this figure. The small dents marked by arrows are not visible on the other generated surfaces, whereas they exist on the true coin surface.

With respect to the fourth item, it is emphasized that special caution is required when evaluating the estimators used to generate figure 4–8.

5 Discussion

This paper deals with arrival time estimation of a narrow-band signal disturbed by white gaussian noise. An estimation method, based on the minimum mean square error criterion, has been examined. Numerical problems with the need of large dynamics in the calculations that showed up have been solved leading to an attractive form of the estimator.

Simulations show that the MMSE-estimator yields, as expected, a smaller mean square error than the MAP-estimator for a wide range of SNRs. For high SNRs the

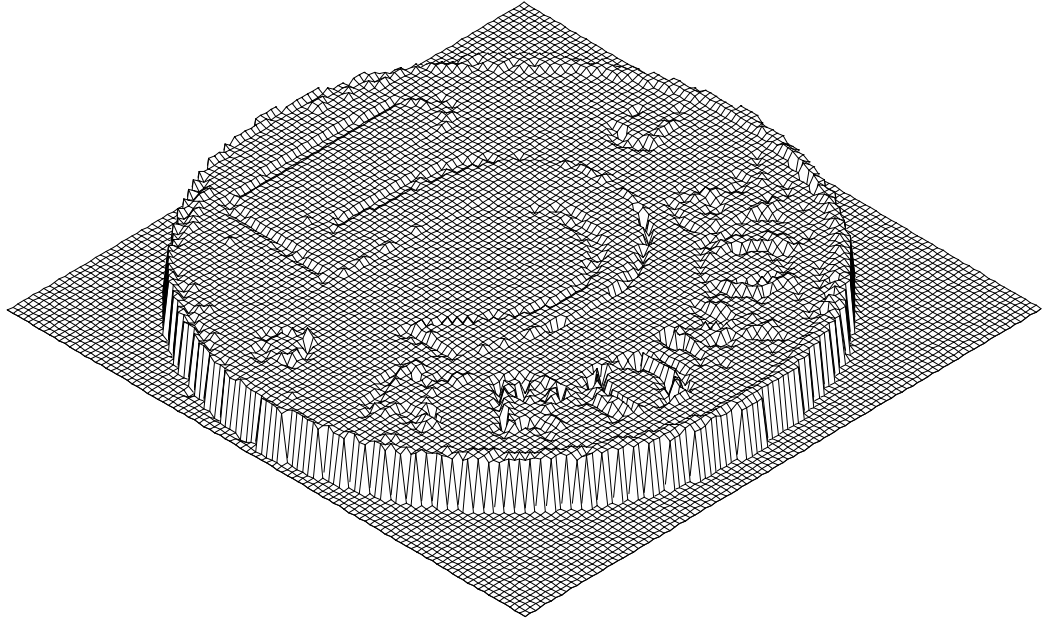


Figure 4: 3D-structure of a coin surface using the MMSE-estimator with $\sigma_D^2 = 228 \text{ [mV]}^2$

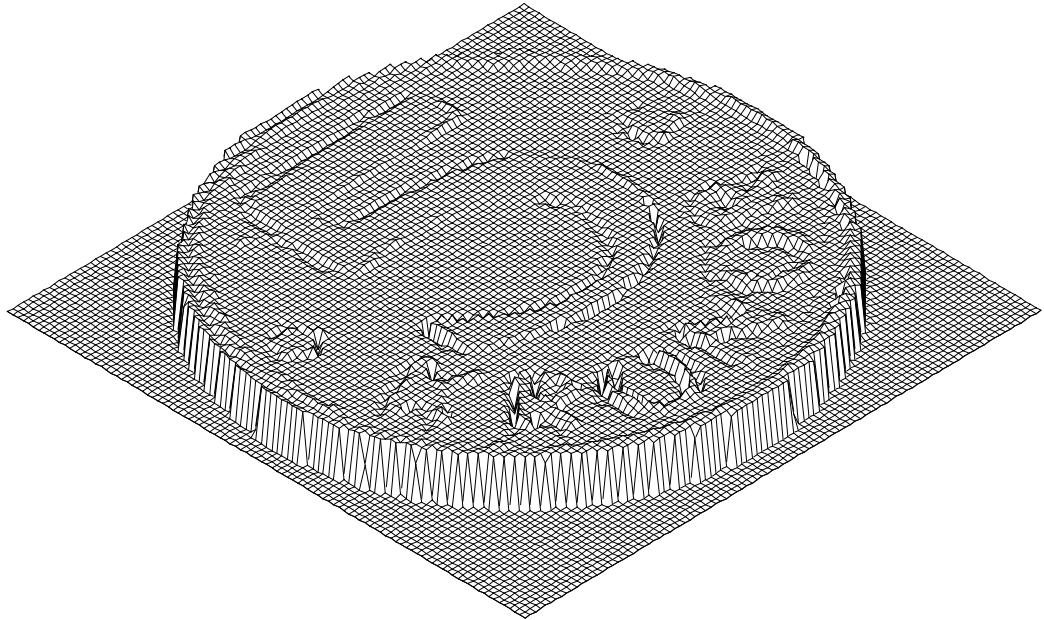


Figure 5: 3D-structure of a coin surface using the MMSE-estimator with $\sigma_D^2 = 6870 \text{ [mV]}^2$

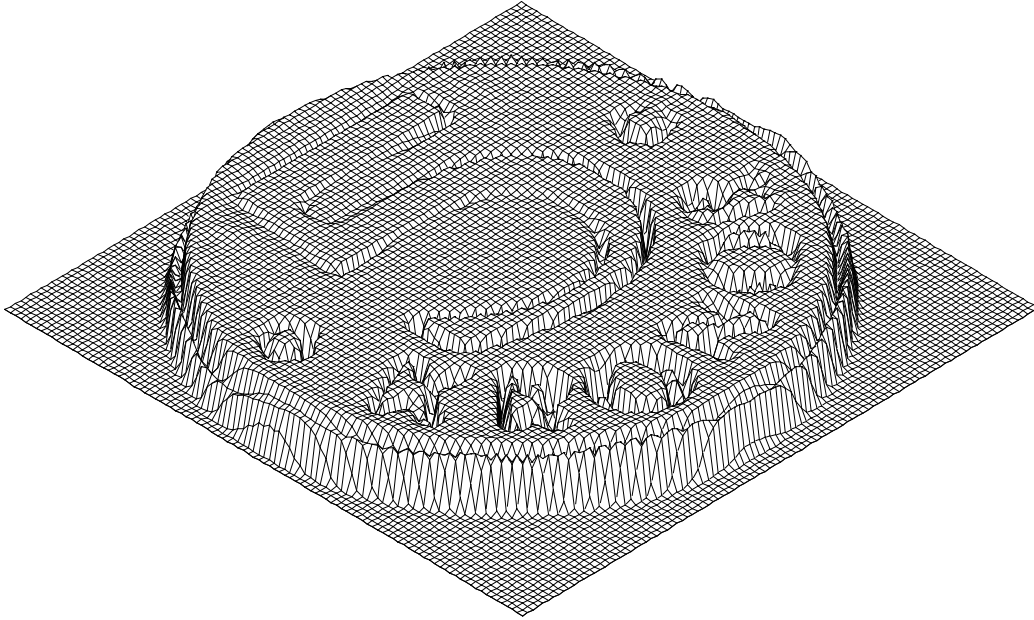


Figure 6: 3D-structure of a coin surface using the MMSE-estimator with $\sigma_D^2 = 68700 \text{ [mV]}^2$

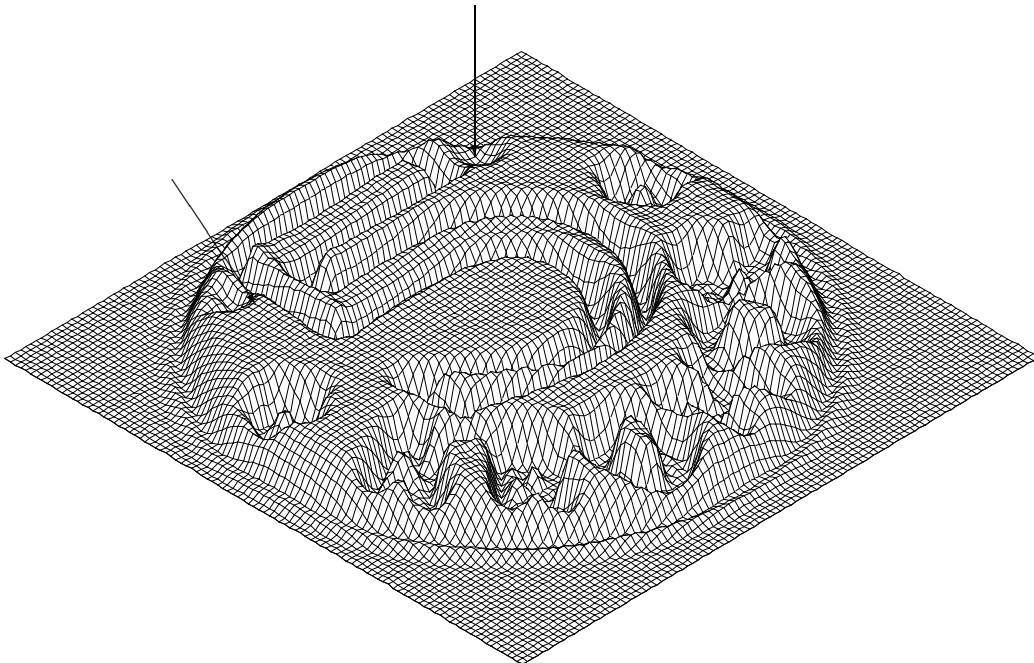


Figure 7: 3D-structure of a coin surface using the MMSE-estimator with $\sigma_D^2 = 687000 \text{ [mV]}^2$

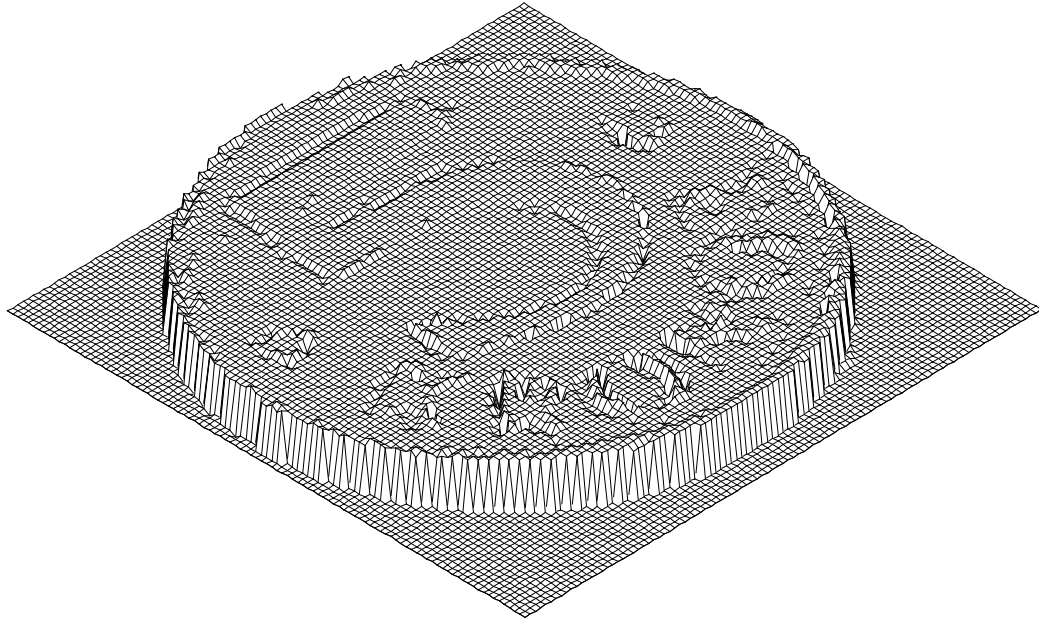


Figure 8: 3D-structure of a coin surface using the MAP-estimator.

MMSE-estimates and the MAP-estimates coincide. Below a critical SNR the MMSE-estimator addresses the peak ambiguity problem by taking into account information contained in adjacent peaks of the correlator output. This is done by averaging over all important correlation peaks which smooths the estimate, thus reducing the peak ambiguity error.

Since the MMSE-estimates and the MAP-estimates almost coincide for high SNRs and the MMSE-estimator deals with the peak ambiguity problem of time delay estimation in situations where the signal to noise ratio does not exceed the threshold SNR, the MMSE-estimator is an attractive alternative to the MAP-estimator. Since the threshold SNR increases as the signal bandwidth decreases, the MMSE-estimator can be of great value in applications dealing with narrow-band systems. Moreover the MMSE-estimator can be used to develop different estimators without knowing the true noise variance. Experiments show that the MMSE-estimator designed for different noise levels can be valuable depending on the particular application requirements.

References

- [1] N.J. Nilsson. On the optimum range resolution of radar signals in noise. *IRE transactions on information theory*, pages 245–253, October 1961.
- [2] C.H. Knapp and G.C. Carter. The generalized correlation method for estimation of time delay. *IEEE Transactions on acoustics, speech and signal processing*, 24(4):320–

327, 1976.

- [3] J.C. Hassab and R.E. Boucher. Optimum estimation of time delay by a generalized correlator. *IEEE Transactions on acoustics, speech and signal processing*, 27(4):373–380, 1979.
- [4] H.L. van Trees. *Detection, estimation and modulation theory*, volume 1. Wiley, USA, 1968.
- [5] J.C. Hassab and R.E. Boucher. Performance of the generalized cross correlator in the presence of a strong spectral peak in the signal. *IEEE Transactions on acoustics, speech and signal processing*, 29(3):549–555, 1981.
- [6] S.K. Chow and P.M. Schultheiss. Delay estimation using narrow band processes. *IEEE Transactions on acoustics, speech and signal processing*, 29(3):478–484, 1981.
- [7] J.N. Bradley and R.L. Kirlin. Delay estimation by expected value. *IEEE Transactions on acoustics, speech and signal processing*, 32(1):19–27, 1984.
- [8] J-O. Gustavsson and P.O. Börjesson. ‘Ankomsttidsskattning av rektangulära pulser i en klass av icke-normalfördelat brus’. In B.O. Rönnang, editor, *Proceedings of RVK 90*, pages 282–288, Chalmers Institute of Technology, Sweden, April 1990. ‘Svenska nationalkommitten for radiovetenskap’.
- [9] J-O. Gustavsson and P.O. Börjesson. A generalized matched filter. In *Proceedings of the third international symposium on signal processing and its applications*, pages 16–22, Gold coast, Australia, August 1992.
- [10] K.L. Kosbar. A lower bound for the error-variance of maximum-likelihood delay estimates of discontinuous pulse waveforms. *IEEE Transactions on information theory*, 38(2):451–457, 1992.
- [11] R.E. Blahut. *Principles and practice of information theory*. Addison–Wesley, New-York, 1987.
- [12] J.P. Ianniello. Time delay estimation via cross-correlation in the presence of large estimation errors. *IEEE Transactions on acoustics, speech and signal processing*, 30(6):998–1003, 1982.
- [13] A. Zeira and Schultheiss P.M. Thresholds and related problems in time delay estimation. In *Proceedings of international conference on acoustics, speech and signal processing*, pages 1261–1264, Toronto, Canada, May 1991. IEEE.
- [14] A.J. Weiss and E. Weinstein. Fundamental limitations in passive time delay estimation – Part 1: Narrowband systems. *IEEE Transactions on acoustics, speech and signal processing*, 31(2):472–486, 1983.
- [15] D. Chazan, M. Zakai, and J. Ziv. Improved lower bounds on signal parameter estimation. *IEEE Transactions on information theory*, 21:90–93, 1975.

- [16] J Ziv and M. Zakai. Some lower bounds on signal parameter estimation. *IEEE Transactions on information theory*, 15(3):386–391, 1969.
- [17] A.J. Weiss and E. Weinstein. A lower bound on the mean-square error in random parameter estimation. *IEEE Transactions on information theory*, 31(5):680–682, 1985.
- [18] A.J. Weiss. Composite bounds on arrival time estimation errors. *IEEE Transactions on aerospace and electronic systems*, 22(6):751–756, 1986.
- [19] Sundström N., Börjesson P.O., Holmer N-G., Olsson L., and Persson H.W. Registration of surface structures using airborne focused ultrasound. *Ultrasound in medicine and biology*, 17(5):513–518, 1991.

Part IV

On Channel Estimation in OFDM Systems

This part has been published as

J.J. van de Beek, O. Edfors, M. Sandell, S.K. Wilson, P.O. Börjesson, ‘On Channel Estimation in OFDM Systems’, In *Proceedings of the 1995 IEEE 45th International Vehicular Technology Conference*, pp 815–819, Chicago, USA, 1995.

On Channel Estimation in OFDM Systems

J.J. van de Beek¹ O. Edfors¹ M. Sandell¹

S.K. Wilson² P.O. Börjesson¹

¹ Div. of Signal Processing
Luleå University of Technology
S-971 87 Luleå, Sweden

² Purdue University
School of Electrical Engineering
1285 Electrical Engineering Bldg
West Lafayette, IN 47907-1285,
USA

Abstract – The use of multi-amplitude signaling schemes in wireless OFDM systems requires the tracking of the fading radio channel. This paper addresses channel estimation based on time-domain channel statistics. Using a general model for a slowly fading channel, we present the MMSE and LS estimators and a method for modifications compromising between complexity and performance. The symbol error rate for a 16-QAM system is presented by means of simulation results. Depending upon estimator complexity, up to 4 dB in SNR can be gained over the LS estimator.

1 Introduction

Currently, *orthogonal frequency-division multiplexing* (OFDM) systems [1] are subject to significant investigation. Since this technique has been adopted in the European digital audio broadcasting (DAB) system [2], OFDM signaling in fading channel environments has gained a broad interest. For instance, its applicability to digital TV broadcasting is currently being investigated [3].

The use of *differential phase-shift keying* (DPSK) in OFDM systems avoids the tracking of a time varying channel. However, this will limit the number of bits per symbol and results in a 3 dB loss in *signal-to-noise ratio* (SNR) [4]. If the receiver contains a channel estimator, multi-amplitude signaling schemes can be used.

In [5] and [6], 16-QAM modulation in an OFDM system has been investigated. A decision-directed channel-tracking method, which allows the use of multi-amplitude schemes in a slow Rayleigh-fading environment is analysed in [5].

In the design of wireless OFDM systems, the channel is usually assumed to have a finite-length impulse response. A cyclic extension, longer than this impulse response, is put between consecutive blocks in order to avoid inter-block interference and preserve orthogonality of the tones [7]. Generally, the OFDM system is designed so that the cyclic extension is a small percentage of the total symbol length. This paper discusses channel estimation techniques in wireless OFDM systems, that use this property of the channel impulse response. Hoeher [6] and Cioffi [8] have also addressed this property.

In Section 2, we describe the system model. Section 3 discusses the *minimum mean-square error* (MMSE) and *least-squares* (LS) channel estimators. The MMSE estimator has good performance but high complexity. The LS estimator has low complexity, but

its performance is not as good as that of the MMSE estimator. We present modifications to both MMSE and LS estimators that use the assumption of a finite length impulse response. In Section 4 we evaluate the estimators by simulating a 16-QAM signaling scheme. The performance is presented both in terms of *mean-square error* (MSE) and *symbol error rate* (SER).

2 System Description

We will consider the system shown in Fig. 1, where x_k are the transmitted symbols, $g(t)$ is the channel impulse response, $\tilde{n}(t)$ is the white complex Gaussian channel noise and y_k are the received symbols. The transmitted symbols x_k are taken from a multi-amplitude signal constellation. The D/A and A/D converters contain ideal low-pass filters with bandwidth $1/T_s$, where T_s is the sampling interval. A cyclic extension of time length T_G (not shown in Fig. 1 for reasons of simplicity) is used to eliminate inter-block interference and preserve the orthogonality of the tones.

We treat the channel impulse response $g(t)$ as a time-limited pulse train of the form

$$g(t) = \sum_m \alpha_m \delta(t - \tau_m T_s), \quad (1)$$

where the amplitudes α_m are complex valued and $0 \leq \tau_m T_s \leq T_G$, i.e., the entire impulse response lies inside the guard space. The system is then modelled using the N -point *discrete-time Fourier transform* (DFT_N) as

$$\mathbf{y} = \text{DFT}_N \left(\text{IDFT}_N(\mathbf{x}) \otimes \frac{\mathbf{g}}{\sqrt{N}} + \tilde{\mathbf{n}} \right) \quad (2)$$

where \otimes denotes cyclic convolution, $\mathbf{x} = [x_0 \ x_1 \ \dots \ x_{N-1}]^T$, $\mathbf{y} = [y_0 \ y_1 \ \dots \ y_{N-1}]^T$, $\tilde{\mathbf{n}} = [\tilde{n}_0 \ \tilde{n}_1 \ \dots \ \tilde{n}_{N-1}]^T$ is a vector of i.i.d. complex Gaussian variables, and $\mathbf{g} = [g_0 \ g_1 \ \dots \ g_{N-1}]^T$ is determined by the cyclic equivalent of sinc-functions. The vector \mathbf{g}/\sqrt{N} is the observed channel impulse response after sampling the frequency response of $g(t)$, and

$$g_k = \frac{1}{\sqrt{N}} \sum_m \alpha_m e^{-j\frac{\pi}{N}(k+(N-1)\tau_m)} \frac{\sin(\pi\tau_m)}{\sin\left(\frac{\pi}{N}(\tau_m - k)\right)}. \quad (3)$$

The validity of the cyclic model described by (2) and (3) depends on how well the objective of the guardspace is met, i.e., how well it eliminates inter-block interference.

If the delay τ_m is an integer, then all the energy from α_m is mapped to tap g_{τ_m} . However, for a non- T -spaced pulse, i.e., if τ_m is not an integer, its energy will leak to all

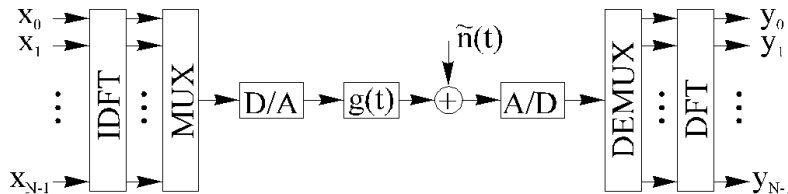


Figure 1: Base-band OFDM system.

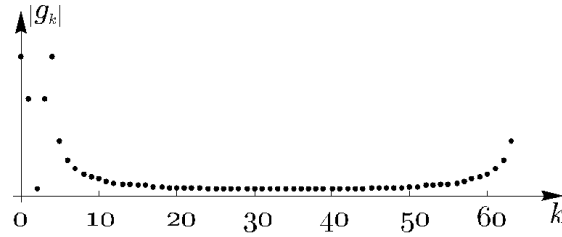


Figure 2: Leakage between taps for the continuous channel $g(t) = \delta(t - 0.5T_s) + \delta(t - 3.5T_s)$.

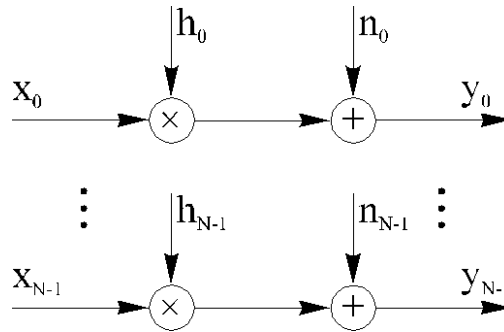


Figure 3: Parallel Gaussian channels.

taps g_k . Fig. 2 illustrates this leakage for a special case. Notice that most of the energy is kept in the neighbourhood of the original pulse locations.

The system described by (2) can be written as a set of N independent Gaussian channels, see Fig. 3,

$$y_k = h_k x_k + n_k, \quad k = 0 \dots N-1, \quad (4)$$

where h_k is the complex channel attenuation given by $\mathbf{h} = [h_0 \ h_1 \ \dots \ h_{N-1}]^T = \text{DFT}_N(\mathbf{g})$ and $\mathbf{n} = [n_0 \ n_1 \ \dots \ n_{N-1}]^T = \text{DFT}_N(\tilde{\mathbf{n}})$ is an i.i.d. complex zero-mean Gaussian noise vector.

As a matter of convenience, we write (4) in matrix notation

$$\mathbf{y} = \mathbf{X}\mathbf{F}\mathbf{g} + \mathbf{n}, \quad (5)$$

where \mathbf{X} is a matrix with the elements of \mathbf{x} on its diagonal and

$$\mathbf{F} = \begin{bmatrix} W_N^{00} & \dots & W_N^{0(N-1)} \\ \vdots & \ddots & \vdots \\ W_N^{(N-1)0} & \dots & W_N^{(N-1)(N-1)} \end{bmatrix} \quad (6)$$

is the DFT-matrix with

$$W_N^{nk} = \frac{1}{\sqrt{N}} e^{-j2\pi \frac{nk}{N}}. \quad (7)$$

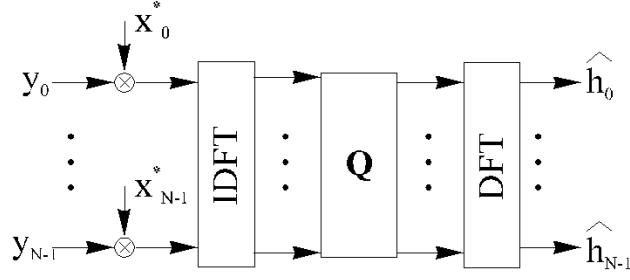


Figure 4: General estimator structure.

3 Channel Estimation

We will derive several estimators based on the system model in the previous section. These estimation techniques all have the general structure presented in Fig. 4. The transmitted symbols x_k , appearing in the estimator expressions, are either training symbols or quantized decision variables in a decision-directed estimator. Error propagation in the decision-directed case is not treated in this paper.

3.1 MMSE and LS Estimators

If the channel vector \mathbf{g} is Gaussian and uncorrelated with the channel noise \mathbf{n} , the MMSE estimate of \mathbf{g} becomes [9]

$$\hat{\mathbf{g}}_{\text{MMSE}} = \mathbf{R}_{\mathbf{g}\mathbf{y}} \mathbf{R}_{\mathbf{y}\mathbf{y}}^{-1} \mathbf{y} \quad (8)$$

where

$$\begin{aligned} \mathbf{R}_{\mathbf{g}\mathbf{y}} &= \text{E} \{ \mathbf{g}\mathbf{y}^H \} = \mathbf{R}_{\mathbf{g}\mathbf{g}} \mathbf{F}^H \mathbf{X}^H \\ \mathbf{R}_{\mathbf{y}\mathbf{y}} &= \text{E} \{ \mathbf{y}\mathbf{y}^H \} = \mathbf{X}\mathbf{F}\mathbf{R}_{\mathbf{g}\mathbf{g}}\mathbf{F}^H\mathbf{X}^H + \sigma_n^2 \mathbf{I}_N \end{aligned}$$

are the cross covariance matrix between \mathbf{g} and \mathbf{y} and the auto-covariance matrix of \mathbf{y} . Further, $\mathbf{R}_{\mathbf{g}\mathbf{g}}$ is the auto-covariance matrix of \mathbf{g} and σ_n^2 denotes the noise variance $\text{E}\{|n_k|^2\}$. These two quantities are assumed to be known. Since the columns in \mathbf{F} are orthonormal, $\hat{\mathbf{g}}_{\text{MMSE}}$ generates the frequency-domain MMSE estimate $\hat{\mathbf{h}}_{\text{MMSE}}$ by

$$\hat{\mathbf{h}}_{\text{MMSE}} = \mathbf{F}\hat{\mathbf{g}}_{\text{MMSE}} = \mathbf{F}\mathbf{Q}_{\text{MMSE}}\mathbf{F}^H\mathbf{X}^H\mathbf{y}, \quad (9)$$

where \mathbf{Q}_{MMSE} can be shown to be

$$\mathbf{Q}_{\text{MMSE}} = \mathbf{R}_{\mathbf{g}\mathbf{g}} \left[(\mathbf{F}^H\mathbf{X}^H\mathbf{X}\mathbf{F})^{-1}\sigma_n^2 + \mathbf{R}_{\mathbf{g}\mathbf{g}} \right]^{-1} (\mathbf{F}^H\mathbf{X}^H\mathbf{X}\mathbf{F})^{-1}. \quad (10)$$

This MMSE channel estimator (9) has the form shown in Fig. 4. If \mathbf{g} is not Gaussian, $\hat{\mathbf{h}}_{\text{MMSE}}$ is not necessarily a minimum mean-square error estimator. It is however the best linear estimator in the mean-square error sense. In either case (\mathbf{g} , Gaussian or not) we will denote the channel estimate as $\hat{\mathbf{h}}_{\text{MMSE}}$.

The LS estimator for the cyclic impulse response \mathbf{g} minimizes $(\mathbf{y} - \mathbf{X}\mathbf{F}\mathbf{g})^H(\mathbf{y} - \mathbf{X}\mathbf{F}\mathbf{g})$ and generates

$$\hat{\mathbf{h}}_{\text{LS}} = \mathbf{F}\mathbf{Q}_{\text{LS}}\mathbf{F}^H\mathbf{X}^H\mathbf{y}, \quad (11)$$

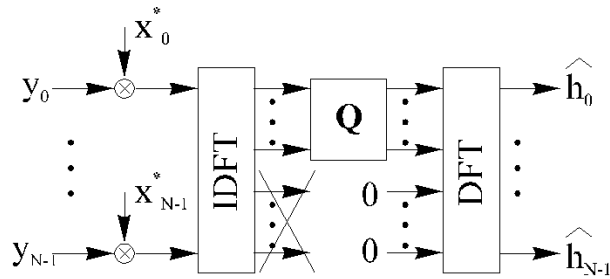


Figure 5: Modified estimator structure.

where

$$\mathbf{Q}_{\text{LS}} = (\mathbf{F}^H \mathbf{X}^H \mathbf{X} \mathbf{F})^{-1} \quad (12)$$

Note that $\hat{\mathbf{h}}_{\text{LS}}$ also corresponds to the estimator structure in Fig. 4. Since (11) reduces to

$$\hat{\mathbf{h}}_{\text{LS}} = \mathbf{X}^{-1} \mathbf{y}, \quad (13)$$

the LS estimator is equivalent to what is also referred to as the zero-forcing estimator.

Both estimators (9) and (13) have their drawbacks. The MMSE estimator suffers from a high complexity, whereas the LS estimate has a high mean-square error. In the next section, we will address these drawbacks and modify both estimators.

3.2 Modified MMSE and LS Estimators

The MMSE estimator requires the calculation of an $N \times N$ matrix \mathbf{Q}_{MMSE} , which implies a high complexity when N is large. A straightforward way of decreasing the complexity is to reduce the size of \mathbf{Q}_{MMSE} . As indicated in Fig. 2, most of the energy in \mathbf{g} is contained in, or near, the first $L = \lceil \frac{T_G}{T_s} \rceil$ taps. Therefore we study a modification of the MMSE estimator, where only the taps with significant energy are considered. The elements in $\mathbf{R}_{\mathbf{g}\mathbf{g}}$ corresponding to low energy taps in \mathbf{g} are approximated by zero.

If we take into account the first L taps of \mathbf{g} , and set $\mathbf{R}_{\mathbf{g}\mathbf{g}}(r, s) = 0$ for $r, s \notin [0, L-1]$, then \mathbf{Q}_{MMSE} is effectively reduced to an $L \times L$ matrix. If the matrix \mathbf{T} denotes the first L columns of the DFT-matrix \mathbf{F} and $\mathbf{R}'_{\mathbf{g}\mathbf{g}}$ denotes the upper left $L \times L$ corner of $\mathbf{R}_{\mathbf{g}\mathbf{g}}$, the modified MMSE estimator becomes

$$\hat{\mathbf{h}}_{\text{MMSE}} = \mathbf{T} \mathbf{Q}'_{\text{MMSE}} \mathbf{T}^H \mathbf{X}^H \mathbf{y} \quad (14)$$

where

$$\mathbf{Q}'_{\text{MMSE}} = \mathbf{R}'_{\mathbf{g}\mathbf{g}} \left[(\mathbf{T}^H \mathbf{X}^H \mathbf{X} \mathbf{T})^{-1} \sigma_n^2 + \mathbf{R}'_{\mathbf{g}\mathbf{g}} \right]^{-1} (\mathbf{T}^H \mathbf{X}^H \mathbf{X} \mathbf{T})^{-1} \quad (15)$$

This modification is illustrated in Fig. 5. As mentioned in Section 1, an OFDM system is usually designed so that L is a small fraction of N . Thus, the complexity of the MMSE estimator will decrease considerably.

Although the complexity of the LS estimator does not prompt for modifications, its performance in terms of mean-square error can be improved for a range of SNRs by following the same general concept as above. The LS estimator does not use the statistics of the channel. Intuitively, excluding low energy taps of \mathbf{g} will to some extent compensate for this shortcoming since the energy of \mathbf{g} decreases rapidly outside the first L taps, whilst the noise energy is assumed to be constant over the entire range [6, 8].

Taking only the first L taps of \mathbf{g} into account, thus implicitly using channel statistics, the modified LS estimator becomes

$$\hat{\mathbf{h}}_{\text{LS}} = \mathbf{T}\mathbf{Q}'_{\text{LS}}\mathbf{T}^H\mathbf{X}^H\mathbf{y} \quad (16)$$

where

$$\mathbf{Q}'_{\text{LS}} = (\mathbf{T}^H\mathbf{X}^H\mathbf{X}\mathbf{T})^{-1}. \quad (17)$$

The modified LS estimator also has the structure as shown in Fig. 5.

3.3 Estimator Complexity

The complexity of the modified LS estimator (16) will be larger than that of the full LS estimator, since a simplification as in (13) cannot be performed. Notice that while the full LS estimator (13) has much lower complexity than the full MMSE estimator (9), the respective modified versions (16) and (14) are equally complex.

It should be noted that the MMSE estimators have been derived under the assumption of known channel correlation and noise variance. In practice these quantities, $\mathbf{R}_{\mathbf{g}\mathbf{g}}$ and σ_n^2 , are either taken fixed or estimated, possibly in an adaptive way. This will increase the estimator complexity and reduce the performance slightly.

In the special case where the channel (1) is T -spaced, i.e., where τ_m are integers, no leakage of energy to taps outside the interval $[0, L]$ will occur and the two modified estimators (14) and (16) will not lose any information about the channel. Thus, the modified MMSE estimator (14) is equivalent to the MMSE estimator (9). The modified LS estimator (16) in this case will outperform the LS estimator (13) for all SNRs, since the excluded taps contain only noise.

More generally, for non- T -spaced channels, any subset of the taps in \mathbf{g} may be taken into account when modifying the MMSE and the LS estimator. The size of this subset determines the complexity for both types of modified estimators.

In Section 4 we consider the case where this subset consists of the taps $g_0 \dots g_{L+K-1}$ and $g_{N-K} \dots g_{N-1}$, i.e., the first L taps as well as K extra taps on each side.

4 Simulations

4.1 Simulated Channels

In the simulations we consider a system operating with a bandwidth of 500 kHz, divided into 64 tones with a total symbol period of 138 μs , of which 10 μs is a cyclic

prefix. Sampling is performed with a 500 kHz rate. A symbol thus consists of 69 samples, five of which are contained in the cyclic prefix (i.e. $L = 5$). 50,000 channels are randomized per average SNR, each consisting of five pulses, of which four have uniformly distributed delays over the interval 0–10 μs , while one tap is always assumed to have a zero delay, corresponding to a perfect time synchronisation of the sampling instants. The multipath intensity profile is assumed to be $\phi(\tau) \sim e^{-\tau/\tau_{\text{rms}}}$, where τ_{rms} is 1/4 of the cyclic extension. We have used Monte-Carlo simulations to generate the \mathbf{R}_{gg} for this channel model. This covariance matrix together with the true noise variance σ_n^2 is used in the MMSE estimations to follow. The average SNR per symbol in Fig. 3 is defined as $E\{|h_k|^2\}/E\{|n_k|^2\}$, since $E\{|x_k|^2\}$ is normalised to unity.

The following estimators are used:

Estimator	Notation	Taps used	Size \mathbf{Q}'
MMSE	MMSE	0...63	64×64
LS	LS	0...63	N.A.
Modified MMSE	MMSE-0	0...4	5×5
	MMSE-5	0...9, 59...63	15×15
	MMSE-10	0...14, 54..63	25×25
Modified LS	LS-0	0...4	5×5
	LS-5	0...9, 59...63	15×15
	LS-10	0...14, 54..63	25×25

4.2 Mean-square Error

Fig. 6 shows the mean-square error versus SNR for the MMSE, LS, MMSE-0, MMSE-5 and MMSE-10 estimators. The difference between the modified MMSE estimators and the MMSE estimator is due to the fact that parts of the channel statistics are not taken into account in the former. For low SNRs, this approximation effect is small compared to the channel noise, while it becomes dominant for large SNRs. The curves level out to a value determined by the energy in the excluded taps. Larger dimensions of \mathbf{Q}'_{M} will give lower mean-square error for all SNRs.

Fig. 7 shows the mean-square error versus average SNR for the MMSE, LS, LS-0, LS-5 and LS-10 estimators. Contrary to the modification of the MMSE estimator, the modification of the LS estimator reduces the mean-square error for a range of SNRs. However, the same approximation effect as in the modified MMSE estimators shows up at high SNRs. An interesting observation is, that for every SNR there exists an optimal size of \mathbf{Q}'_{LS} , which gives the smallest mean-square error compared to the other modified LS estimators.

4.3 Symbol-error Rate

The symbol-error rate (SER) curves presented in this section are based on the mean-square errors of the channel estimations presented in the previous section. For the calculation of SER, we have used the formulae presented in [10]. These formulae find the

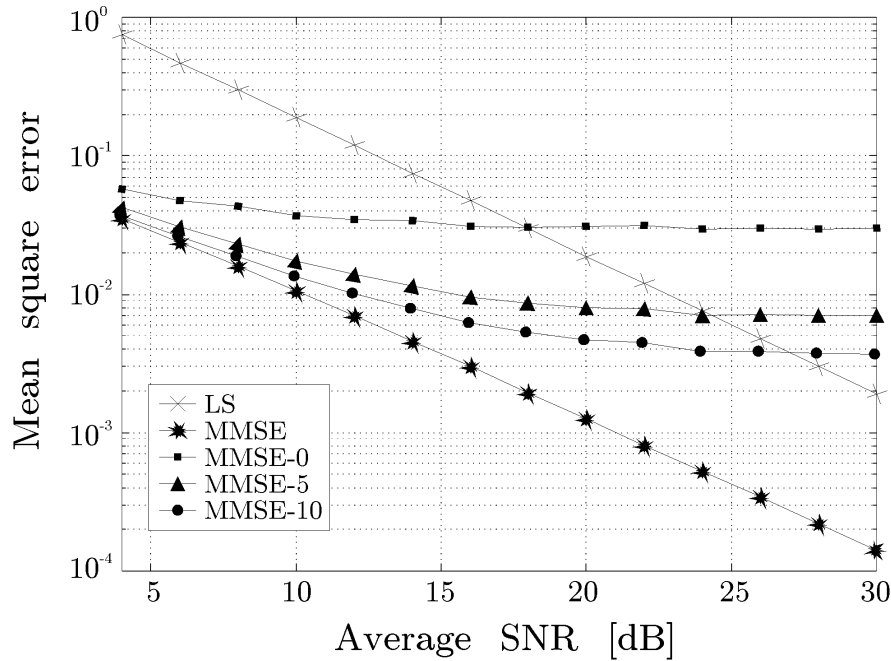


Figure 6: Mean-square error for three modified MMSE estimators.

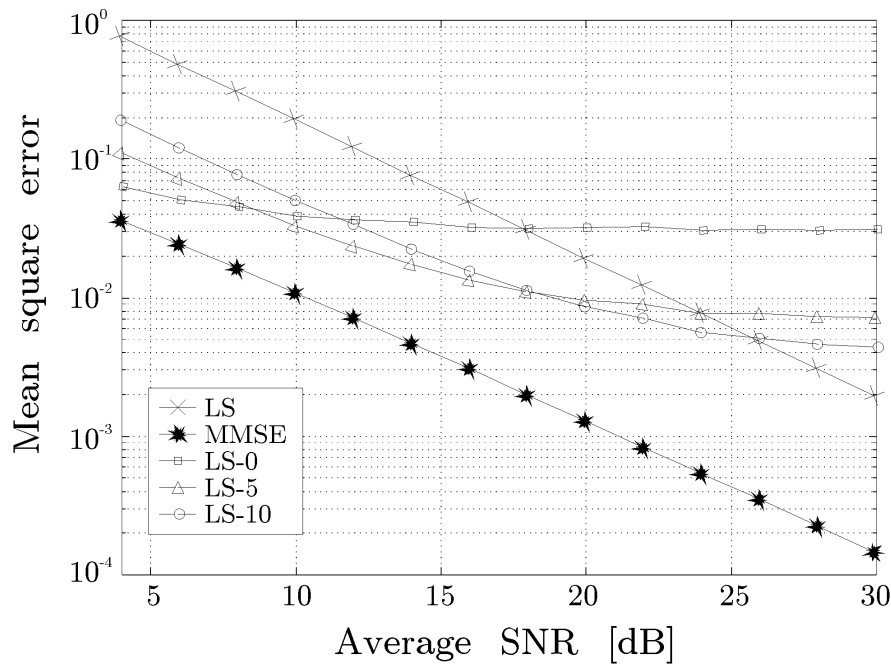


Figure 7: Mean-square error for three LS estimators.

symbol error rate of a 16-QAM system given a noisy estimate of the channel. We consider decision-directed estimation, without error propagation.

As seen in Fig. 8, a gain in SNR up to 4 dB can be obtained for certain SNRs when using a modified MMSE estimator instead of the LS estimator, depending on admissible complexity. The same behaviour can be observed for modified LS estimators in Fig. 9.

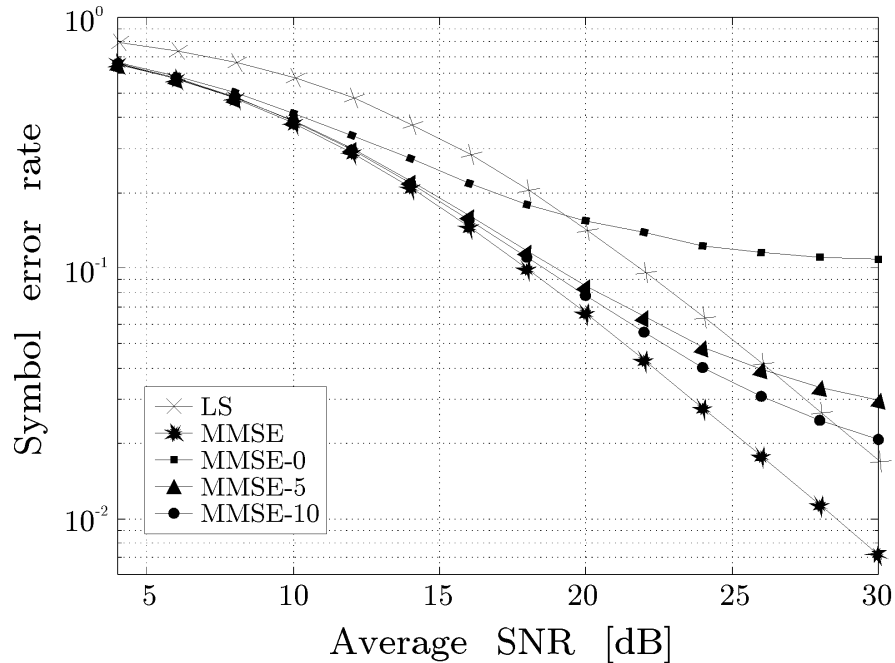


Figure 8: Symbol error rate for three modified MMSE estimators.

However, the gain in SNR is not as large as for the modified MMSE estimators with the same size of the matrix \mathbf{Q} . This is explicitly shown for MMSE-10 and LS-10 in Fig. 10. The difference in SNR between these two estimators is about 2 dB.

5 Conclusions

The estimators in this study can be used to efficiently estimate the channel in an OFDM system given a certain knowledge about the channel statistics. The MMSE estimator assumes *a priori* knowledge of noise variance and channel covariance. Moreover, its complexity is large compared to the LS estimator. For high SNRs the LS estimator is both simple and adequate. However, for low SNRs, the presented modifications of the MMSE and LS estimators will allow a compromise between estimator complexity and performance. For a 16-QAM signaling constellation, up to 4 dB gain in SNR over the LS estimator was obtained, depending on estimator complexity. Even relatively low-complex modified estimators, however, perform significantly better than the LS estimator for a range of SNRs.

References

- [1] Leonard J. Cimini, Jr., "Analysis and simulation of a digital mobile channel using orthogonal frequency-division multiplexing", *IEEE Trans. Comm.*, Vol. 33, no. 7, pp 665–675, July 1985.

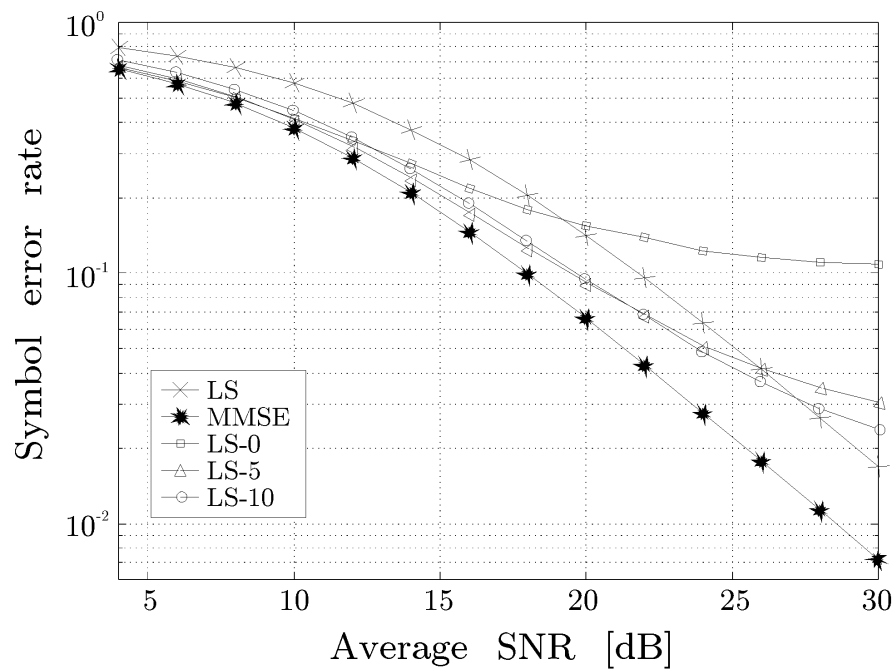


Figure 9: Symbol error rate for three modified LS estimators.

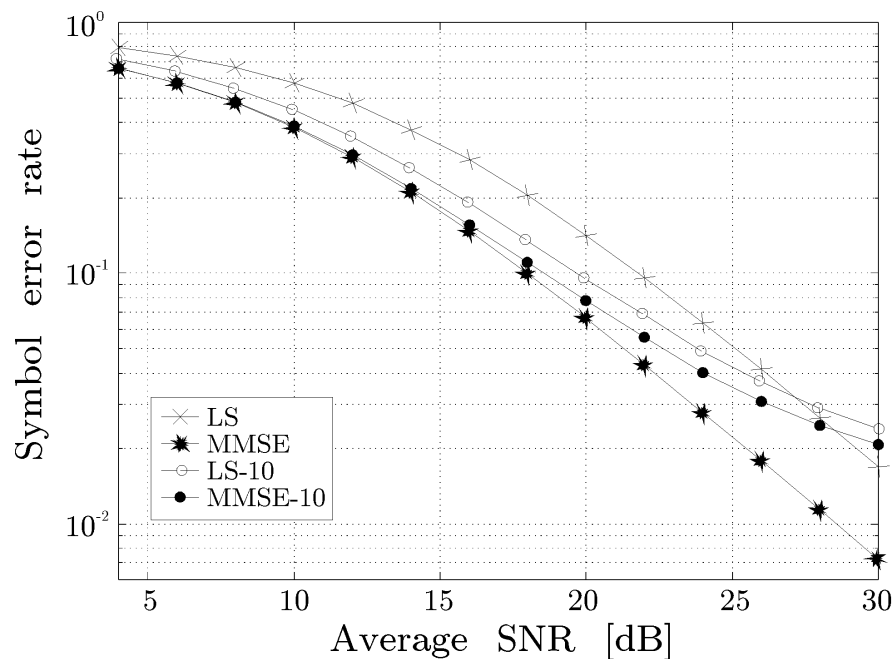


Figure 10: Comparison of SER between a modified MMSE estimator and the corresponding modified LS estimator.

[2] M. Alard and R. Lassalle, “Principles of modulation and channel coding for digital broadcasting for mobile receivers”, *EBU Review*, no. 224, pp 3–25, August 1987.

[3] B. Marti et al., “European activities on digital television broadcasting—from com-

pany to cooperative projects”, *EBU Technical Review*, no. 256, pp. 20–29, 1993.

- [4] John Proakis, *Digital Communications*, McGraw-Hill, 1989.
- [5] Sarah Kate Wilson, R. Ellen Khayata and John M. Cioffi, “16-QAM modulation with orthogonal frequency-division multiplexing in a Rayleigh-fading environment”, In *Proc. VTC-1994*, pp. 1660–1664, Stockholm, Sweden, June 1994.
- [6] Peter Hoeher, “TCM on frequency-selective land-mobile fading channels”, In *Proc. of the 5th Tirrenia International Workshop on Digital Communications*, Tirrenia, Italy, September 1991.
- [7] John A.C. Bingham, “Multicarrier modulation for data transmission: an idea whose time has come”, *IEEE Communications Magazine*, 28(5):5–14, May 1990.
- [8] John M. Cioffi, Stanford University, Private communication.
- [9] Louis L. Scharf, *Statistical Signal Processing*, Addison–Wesley, 1991.
- [10] Sarah Kate Wilson, Digital Audio Broadcasting in a Fading and Dispersive Channel, PhD-thesis, Stanford University, August 1994.

Summary

Summary

The previous 4 parts were written independently, each addressing a particular problem. The following items summarize and restate the more important results and conclusions in this thesis:

- The simultaneous ML estimator of timing and frequency offset in OFDM systems basically consists of a complex correlator and a moving sum, generating a signal $\gamma(\cdot)$. The estimate of the timing offset is the argument maximizing the (energy-compensated) magnitude of $\gamma(\cdot)$. The estimate of the frequency offset is proportional to the phase of $\gamma(\cdot)$ at this time instant.
- When considering only the sign bits of the in-phase and quadrature components of the received OFDM signal, the ML estimator for the timing offset consists of a complex correlator and a moving sum, followed by a peak detector. The complexity of this estimator is small compared to the ML estimator based on the received signal represented with full resolution.
- Simulations show that the performance of the frequency estimator is applicable in a tracking mode while the timing estimation can be used in an acquisition mode. The low-complex method, combined with an averaging step, may be used in a tracking mode, depending on the system requirements
- The MMSE estimator of time delay, where the transmitted signal is deterministic and known, is more robust to the peak ambiguity problem than the MAP estimator. Numerical problems concerning the necessity for large dynamics in the calculations can be solved, leading to an implementationally attractive form of the estimator.
- In an airborne ultrasound measuring system, the MMSE-estimator of time delay can be used to develop different modified estimators without knowing the true noise variance. These modified estimators, designed for different noise levels, may be valuable depending on the particular application.
- In OFDM systems with up to 20 dB in signal-to-noise ratio, the complexity of the linear MMSE and LS channel estimators (in terms of number of multiplications) can be decreased considerably without losing much in performance. When considering the symbol error rate in an uncoded, 16-QAM OFDM system, up to 4 dB in SNR can be gained over the LS estimator, depending on estimator complexity. No more than 1 dB loss in SNR compared to the linear MMSE channel estimator needs to be sacrificed.